2013

Predicting mechanical properties of southern pine lumber with nondestructive measurements

Jacob Romer
Louisiana State University and Agricultural and Mechanical College

PREDICTING MECHANICAL PROPERTIES OF SOUTHERN PINE LUMBER WITH NONDESTRUCTIVE MEASUREMENTS

A Thesis

Submitted to the Graduate Faculty of the
Louisiana State University and
Agricultural and Mechanical College
in partial fulfillment of the
requirements for the degree of
Master of Science

in

The School of Renewable Natural Resources

by
Jacob Romer
B.S., State University of New York
College of Environmental Science and Forestry, 2011
December 2013

ACKNOWLEDGEMENTS

Many people contributed to the completion of this thesis. First, I would like to thank my advisor and committee chair Todd Shupe for giving me the opportunity to continue my studies in graduate school and helping me with whatever I needed to complete this thesis. Also, Jay Curole, who was always willing to help around the lab and shop.I would like to thank Chung-Yun Hse for all of his advice and making me feel at home in Pineville. I would also to thank all the other employees and scientists at the USDA Forest Service Southern Research Center in Pineville, LA., especially Donna Edwards who helped me with many things. Thanks to Neils de Hoop for being part of my committee and providing suggestions for the preparation of the thesis and helping to make it as good as possible. Also, a special thanks to Neal Hickman. Without his knowledge and help, setting up the testing equipment would have been impossible and this may have never been completed. Last but not least, a thanks to my family and friends for all the love and support.

TABLE OF CONTENTS

LIST OF TABLES

LIST OF FIGURES

ABSTRACT

Predictive models were developed for stiffness and bending strength of southern pine 2x6, eight ft. lumber using nondestructive measurements of stresswave velocity, density and visual characteristics such as knots, slope of grain and rate of growth. To account for local areas of weakened material due to knots and slope of grain, a grid system was developed to quantify general knot size and location. Multiple regression models were created using these physical and visual measurements. Two sets of models were developed: one that removed influential samples with abnormal wavespeeds (greater than 18,000 ft./s) indicative of poor wood quality; and, models that included all samples. Static modulus of elasticity (MOE_s) model performance was significantly better for those that removed influential samples compared to the all-sample models, with an R^2 of 0.892 and 0.720, respectively. Modulus of rupture (*MOR*) model performance was slightly better with influential samples removed – R^2 of 0.714 and 0.690, respectively. The location of knots within a board significantly altered the mechanical properties, especially bending strength. The results indicate potential for greater specification of allowable stresses for different orientations during bending. A simulated grading study was conducted to assess the feasibility of the developed models. Thousands of samples were generated according to estimated variable distributions and graded according to the American Lumber Standards Committee Machine Graded Policy. Results suggest that these models may be feasible in an actual lumber grading scenario.

1. INTRODUCTION

1.1 Introduction

Accurate knowledge of the mechanical properties of structural lumber is essential for the proper and efficient use of the material. Unlike most engineering materials, wood is produced by a living organism and, as a result, is highly variable due to environmental conditions, genetic factors and growth variations (Panshin and DeZeuw 1980). Due to this uncertainty of the material properties, a range of methods have been developed to predict the properties of wood using indirect observation - that is, measurements obtained without permanently damaging or altering the properties of the material (Table 1.1). Nondestructive evaluation (NDE) technologies have greatly improved prediction of wood properties which has led to improved grading practices and increased standardization according to strength and stiffness. Correct classification of lumber is imperative not only for the reliability of a structure, but for the benefit of both producers and users of lumber. Improved prediction of mechanical properties reduces variability within a grade and allows each piece to be placed in categories with narrower distribution and may even be sorted specific applications in mind (FPL 2010).

Table 1.1 – Nondestructive tests to determine wood properties (Ross et al. 1998)

Visual Characteristics	color, defects, slope of grain
Physical Tests	electrical resistance, dielectric properties, vibrational properties, wave propagation, acoustic emissions, x-ray, NIR spectroscopy
Chemical Tests	composition, presence of treatments
Mechanical Tests	flexural stiffness, proof loading, cores

1.2 Lumber Grading Overview

Visual grading of structural lumber is the oldest and most widely-used method for the prediction of mechanical properties. In 1923, the USDA Forest Service Forest Products Laboratory published a set of basic grading rules with the first assigned stress values for structural lumber. Growth characteristics present in lumber identified by the naked eye such as knots, slope of grain, checks and splits, shake, density, decay, and wane are used to estimate the reduction in mechanical properties from clear wood of that species. Penalties from clear wood properties, called strength ratios and quality factors for stress and stiffness, respectively, are empirically or theoretically derived for each growth defect. Depending on the knot size and location, for instance, various reductions in strength and stiffness are applied to clear wood values which are then translated to full-size structural lumber. Several limiting growth defects may be present in a sample, but the greatest reduction is used to estimate the strength according to ASTM D245 – 06 (ASTM 2011).

Visually methods have been sufficient in grading structural lumber, primarily for the purpose of light framing in residential structures. Mechanically (or machine) graded lumber has become widely used for certain applications, such as metal plate trusses or laminated beams, and allows the development of increased yield of grades similar to visual grades (Galligan and McDonald 2000). Machine stress-rated (MSR) lumber and machine-evaluated lumber (MEL) are two methods which both use predictor variables to find the relationship with mechanical properties using regression or other statistical inference techniques. Strength-reducing growth characteristics used in visual grading, such as edge knots, are incorporated into machine grading criteria to further improve prediction. Unlike visual grades that require unique grade rules for each specie, machine

graded lumber and its design values are based on physical measurements of the individual board which are generally independent of species. Variation within machine grades are generally less than comparable visual grades, also.

1.3 Southern Pine Lumber

The four major southern pines – Loblolly, Longleaf, Slash and Shortleaf – are among the most widely used and versatile wood species in North America. Their individual ranges overlap and extend from the upper areas of the south Atlantic states across the southern states to Texas and Oklahoma. Southern pine is strong, dries rapidly, treats easily with chemicals and, most importantly, is ideal for residential construction. Southern pine has some the highest allowable design values of all North American softwood species and is an extremely important engineering material (FPL 2010; AWC 2012).

Following the peak of 19.0 billion board feet of production in 2005 and the subsequent downturn of the housing market, a full recovery is expected by 2014 and the demand for southern pine structural lumber will most likely increase. In particular, demand for MSR/MEL southern pine lumber is projected to increase substantially over the next five to seven years due to decreased supply capacity of spruce-pine-fir (SPF) MSR lumber in eastern and western Canada (MSR Lumber Producers Council 2012, 2013b). One cause is the mountain pine beetle in British Columbia which has greatly reduced the volume of merchantable lodgepole pine, a major source of SPF MSR lumber. Several bills in Quebec are also expected to reduce the annual allowable cut (AAC) in Canada. Bill 57, a sustainable forestry measure implemented in 2013, is expected to reduce the AAC by 11.5% while Plan Nord, an economic initiative plan, may reduce the AAC in Quebec by an estimated 6% (MSR Lumber Producers Council 2012, 2013b).

The use of prefabricated components and trends toward optimum value engineering coupled with reductions in design values of visually graded southern pine is expected to cause an increase in the demand and production of machine graded southern pine. By 2017, southern pine MSR lumber is expected to account for over 35% of all machine-graded lumber, up from 21% in a 2012 production survey (MSR Lumber Producers Council 2013a). Increased demand for machine-graded southern pine presents an opportunity to develop new or improved grading techniques.

Of all the dimensions of southern pine machine-graded lumber produced in 2012, 2x6 boards were the most produced compared to 2x4, 2x8, 2x10 and 2x12 (Table 1.2). In 2012, MSR lumber production dwarfed MEL southern pine production for 2x6 lumber with MEL at just 2.8 %. However, the percent of MEL lumber within all machine-graded lumber increases as dimension increases (Table 1.2). With less machine-graded SPF available in the coming years, these proportions may change and lead to an increase in smaller dimension MEL southern pine.

Table 1.2 – Machine-stress rated and machine evaluated southern pine lumber production, 2012 (MSR Lumber Producers Council 2013a)

Dimension	Production Volume (MMBF)	Percent of Total SYP Production	Percent MEL
2 x 4	59.40	24.15	0
2 x 6	63.39	25.77	2.8
2 x 8	57.35	23.32	10.31
2 x 10	44.64	18.15	22.13
2 x 12	21.17	8.61	28.01

Production data comes from a voluntary survey of 29 MSR lumber producers representing about four dozen North American mills and was conducted by the MSR Lumber Producers Council

as part of its 2012 Annual Production Survey. The relatively small volume of MEL lumber produced is not necessarily indicative of an inferior process as compared to MSR lumber, but could be reflective of the mills and lumber producers involved in the survey. The percent of MEL 2x6 southern pine was well above 10 % of the total machine-graded lumber produced in the past decade (Table 1.3) and may increase in the future.

Table 1.3 – Southern pine 2x6 machine-evaluated lumber (MEL) and machine-stress rated lumber production since 2003, in MMBF (MSR Lumber Producers Council 2013a)

Production Year	2003	2004	2005	2006	2007	2008	2009	2010	2011	2012
MEL Production	11.97	8.34	12.55	9.71	6.1	5.34	3.71	5.55	1.39	1.76
MSR Production	51.40	65.29	72.55	69.68	48.94	43.38	31.09	30.65	39.26	61.63

1.4 References

American Society for Testing and Materials (ASTM). 2011. Standard practice for establishing structural grades and related allowable properties for visually graded lumber. ASTM D245-06 (2011). *In*: Annual Book of ASTM Standards. ASTM, West Conshohocken, Pennsylvania.

American Wood Council (AWC). 2012. National design specification® (NDS®)for wood construction. Leesburg, Virginia.

Forest Products Laboratory (FPL). 2010. Wood handbook – wood as an engineering material. General Technical Report FPL-GTR-190. Madsion, WI: U.S. Department of Agriculture, Forest Service, Forest Products Laboratory.

Galligan, W. L. and K. A. McDonald. 2000. Machine grading of lumber—Practical concerns for lumber producers. Gen. Tech. Rep. FPL–GTR–7 (Revised). Madison, WI: U.S. Department of Agriculture, Forest Service, Forest Products Laboratory.

MSR Lumber Producer's Council. 2012. MSR forecast summary: September 2012. Madison, Wisconsin.

MSR Lumber Producer's Council. 2013a. Annual Production Survey 2012. Madison, Wisconsin.

MSR Lumber Producer's Council. 2013b. MSR forecast summary: first quarter 2013. Madison, Wisconsin.

Panshin, A. J. and C. de Zeeuw. 1980. Texbook of Wood Technology, 4th ed. McGraw-Hill, New York.

Ross, R. J., B. K. Brashaw, and R. F. Pellerin. 1998. Nondestructive evaluation of wood. *Forest Prod. J.* 48(1):14-19.

2. LITERATURE REVIEW

2.1 Nondestructive Evaluation of Lumber

The predictive capability of nondestructive evaluation (NDE) technology has been widely studied over the past century with applications in all phases of the manufacturing process, from assessing the properties of standing trees to monitoring the quality of finished products. A brief overview of visual grading and machine grading of lumber, the two broad categories for predicting mechanical properties, were outlined in Chapter 1. A more detailed account of past work of NDE and its relevance to this study will be outlined.

2.1.1 Static Bending Techniques

The first works in finding the relationship between modulus of rupture (*R*) and modulus of elasticity (*E*) were carried out by Potlatch Forests, Inc. researchers in the early 1960s (Hofstrand and Howe 1960; Glover 1962; Hoerber 1962). Samples were loaded in flatwise bending and regression coefficients were calculated. The difference in calculated modulus of elasticity, whether obtained by flat or edgewise bending, was found to be negligible. Other organizations instrumental in developing the first industrial methods of stress-grading were the Western Pine Association (Portland, Oregon), Commonwealth Scientific and Industrial Research Organization (Melbourne, Australia) and the Timber Research Unit of the Council for Scientific and Industrial Research in South Africa (Galligan and MacDonald 2000). An extensive USDA Forest Products Laboratory study using thousands of southern pine samples conducted by Doyle and Markwardt (1966) further validated an already solid understanding of the relationship of nondestructive parameters and mechanical properties. Among the key findings were that the correlation coefficient of edgewise

E to flatwise *E* was 0.945 and the correlation between *R* (edgewise) and *E* (flatwise) based on linear regression was fairly high – 0.679 for 2 x 4 lumber, 0.607 for 2 x 6, 0.674 for 2 x 8 and 0.443 for 2 x 10.

In an industrial setting in which production speed is critical, lumber grading is a continual process. Boards are fed continuously through the grading machine and held between roller supports with a force applied between them (Figure 2.1). The machine measures either the applied load required to produce a fixed deflection or the deflection under a fixed applied load across any approximately four foot span. The apparent *E*, or deflection relating to stiffness, can then be calculated for various sections across the length of the board. The minimum apparent *E* of any measured span or the average *E* of the entire board may be used to classify the stiffness (FPL 2010). There are numerous varieties of stress-grading machines, each with different loading and roller support mechanisms, board orientation and deflection measurement systems. However, they each utilize the same underlying theory of measuring the apparent *E* to predict other mechanical properties to segregate into grades.

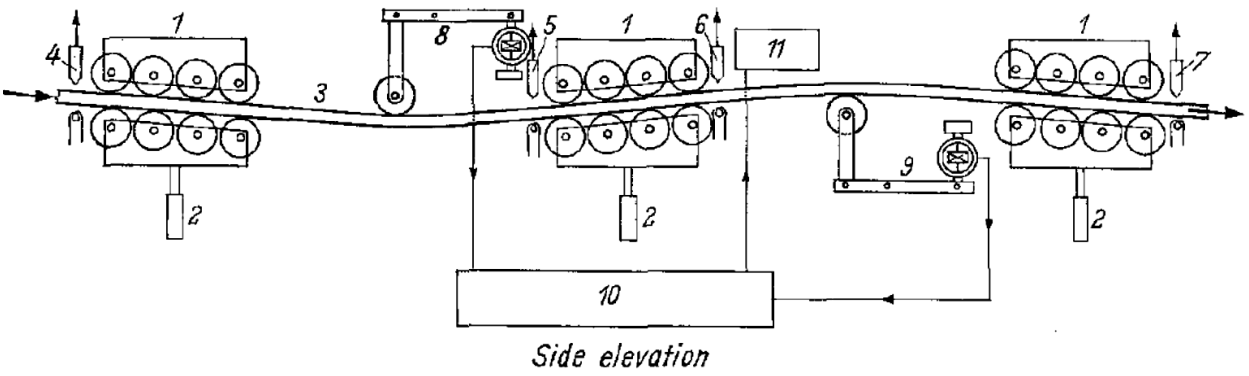

Figure 2.1 – Continuous Lumber Tester manufactured by Industrial Sciences, a common type of grading machine (Muller 1968)

2.1.2 Transverse Vibration Techniques

Vibration methods to predict static properties have been investigated since the 1950s (Kitazawa 1950; Bell et al. 1950; Fukada 1950; Matsumoto 1962). Jayne (1959) explicitly

proposed a fundamental hypothesis of NDE of wood with regards to dynamic methods: the energy storage and dissipation properties of wood materials are controlled by the same mechanisms that determine the static behavior. At the microscopic level, energy storage properties, measured as frequency of oscillation, are related to cellular orientation and material composition. Energy dissipation, measured by rate of decay, is controlled by internal friction characteristics, which is related to bonding behavior between constituents (Ross and Pellerin 1994). The natural frequency of vibration of an object serves as an indication of the energy storage and the logarithmic decay is a measure of the energy dissipation. Jayne hypothesized that energy storage was related to the modulus of elasticity and energy dissipation was related to modulus of rupture (Jayne 1959).

The relationship between dynamic *E* and static *E* was further validated and improved (Jayne 1959; James 1964; Pellerin 1965) but the relationship between energy dissipation and ultimate strength had not been verified until Pellerin (1965) accurately estimated the modulus of rupture by incorporating the energy dissipation of the material, represented by the damping coefficient expressed as the rate of decay of vibrations, also known as the logarithmic decrement. Using the ratio of dynamic *E* over logarithmic decrement to predict MOR on construction lumber of various moisture contents, sizes, and grades, correlation coefficients as high as 0.92 were reported. Among the many recent studies to utilize transverse vibration, Wang et al. (2008) predicted the static *E* from dynamic *E* for 2x4 southern pine with an R^2 of 0.87.

2.1.3 Stress Wave Techniques

Stress wave techniques for the evaluation of wood properties have been used since the late 1800s. Ihlseng (1878, 1879) measured the stress-wave propagation speed of several wood species and was able to calculate the modulus of elasticity. Galligan and Courteau (1965) predicted the

static bending moduli of Douglas-fir 2x6 lumber from the dynamic modulus of elasticity (E_d) obtained from both longitudinal stress wave propagation and transverse vibrational techniques. They reported a 0.966 correlation between E_d obtained from stress waves and transverse vibration, concluding that the stress wave technique was preferred because it was faster and avoided the issue of specimen support that is so critical to vibrational methods.

Numerous studies and reviews have concluded that longitudinal stress waves are an accurate and rapid technique, whether produced through mechanical impact or with piezoelectric transducers operating at higher frequencies of nominal frequency of 20 to 500 kHz (Gerhards 1982; Ross and Pellerin 1994). Sandoz (1989) produced good results for relating dynamic *E* from ultrasonic measurements and density to static *E* from third-point bending tests for spruce beams of varying dimensions. Rajeshwar et al. (1997) predicted the tensile strength of southern pine lumber using ultrasonic methods that were able to detect edge knots as well as slope of grain. Divos and Kiss (2010) developed a portable lumber grading tool that utilized ultrasonic measurement and several other variables to predict bending strength and stiffness of larch lumber.

2.1.4 Other Nondestructive Techniques

A number of other NDE techniques have been researched for the testing of wood products, such as microwave, electrical capacitance, light scattering and radiation. Each technique has its own unique strengths and limitations and is particularly useful in one aspect of determining wood quality. Most applicable and widely used in the grading of structural lumber are those that measure slope of grain. The effect of slope of grain has been investigated thoroughly (Bodig and Jayne 1982; FPL 2010) and is addressed in both SPIB grade rules and AWC NDS®. Two methods of measuring the slope of grain are most prominent: electrical capacitance and light scattering.

The dielectric properties of wood and the effect of anisotropy have been known for many years (Yavorski 1951; Hearmon and Burcham 1954; Peterson 1960; Norimoto and Yamada 1972). In the early 1970s, McLaughlan et al. developed a noncontact slope-of-grain indicator to measure grain angle of a wood product by measuring capacitance. The material is subjected to an electrostatic field and the dielectric constant is measured. McDonald and Bendtsen (1986) measured electrical capacitance on quarter-inch sections to obtain a localized slope of grain profile across the entire board.

Another more practical way to measure slope of grain is light scattering. A laser is directed at the wood surface and is split into reflected light and transmitted light, which travels across either cell walls or cell lumens. During light propagation, light transmitted across cell walls attenuates more than light transmitted across lumens so it is possible to determine cell orientation from how the light propagates – called the "tracheid effect." This phenomenon was explored and technology was developed in the 1980s by Matthews (1987) and Soest (1987), among others.

2.2 Grading of Southern Pine Lumber

2.2.1 Visually-Graded Lumber

Southern pine structural lumber is graded according to the visual grade rules published by the Southern Pine Inspection Bureau (SPIB) in *Standard Grading Rules for Southern Pine Lumber* (SPIB 2002). As mentioned in Chapter 1, growth characteristics identified visually such as knots, slope of grain, rate of growth, checks and splits, shake, density, decay, and wane are used to estimate the reduction in mechanical properties from clear wood. Assigned stress and modulus of elasticity values are based on tests of full-size lumber and/or small clear specimens following the procedures in ASTM D1990 Standard Practice for Establishing Allowable Properties for Visually Graded Dimension Lumber from In-Grade Tests of Full Size Specimens (ASTM 2007), ASTM D

2555 Standard Test Methods for Establishing Clear Wood Strength Values (ASTM 2011) and ASTM D245 Standard Practice for Establishing Structural Grades and Related Allowable Properties for Visually Graded Lumber (ASTM 2011).

Limiting growth characteristics are given for each grade; hence, the rules describe the poorest pieces permitted in a grade, although five percent below grade is the tolerance between graders. Any piece that contains characteristics which exceed those permitted in the grade, even if taken individually is permitted, must be excluded from the grade. As the assigned allowable strength and stiffness increases by grade, the location and magnitude of characteristics become more stringent. In a relatively high grade – Select Structural (average E = 1,800,000 psi, allowable bending stress = 2,100 psi) – sound knots at the edge wide face of 6 inch wide lumber are permitted and are not to exceed 1 and 1/8 inches with slope of grain limited to 1 in 12. For Grade No. 2 (average E = 1,400,000 psi, allowable bending stress = 1,000 psi), sound knots at the edge wide face are not to exceed 1 and 7/8 inches and slope of grain is limited to only 1 in 8.

2.2.2 Mechanically-Graded Lumber

Mechanically graded southern pine is grouped into two broad categories: machine stress rated (MSR) lumber and machine evaluated lumber (MEL). Both are based on the use of physical, mechanical or visual predictors that are related to mechanical properties, mainly modulus of elasticity and bending strength. Minimal information could be found on the approved grading machines used for grading southern pine lumber (Table 2.1). The technology used for each machine is proprietary information and the accuracy and variability of the process used for each is unknown. The Weyerhaeuser RE-I, RE-II and RE-III machines (formerly called "Thumper Strength Grader") most likely utilize stresswaves or vibrational technique and possibly slope-of-grain measurement. The Gradescan®-Based Strength Grading System is an advanced scanning

system that can employ up to five sensors – color, geometric profile, throughboard, tracheid and grain angle – to detect various growth and geometric defects. The Gradescan® lumber scanner uses information from a strength tester or other devices and uses it for its grading decision.

In order to be approved by the American Lumber Standards Committee (ALSC), each applicant must submit evidence that the machine is capable of segregating lumber into appropriate grades, supported by statistical analysis. In addition, an accredited grading agency, such as the SPIB, must submit quality control procedures in order to obtain grade stamps for lumber produced by the grading machine (ALSC 2013).

Table 2.1 – Lumber grading machines approved by the American Lumber Standards Committee Board of Review, supported by the Southern Pine Inspection Bureau

Grading Machine	Machine Manufacturer
X-Ray Lumber Gauge	Newnes Machine Ltd. Company
RE-I	Weyerhaeuser
RE-II	Weyerhaeuser
RE-III	Weyerhaeuser
Weyerhaeuser NR Company's Gradescan®-Based Strength Grading System	Weyerhaeuser/Lucidyne Technologies Gradescan

In order for a grading agency to qualify a machine grade, they are required to verify that the grade to be qualified meets the following minimum criteria:

For MSR lumber:

(1) Average edge modulus of elasticity (*MOE*) equal to or greater than the assigned average *E;*

(2) 95% of pieces have edge *MOE* greater than 82% of assigned average *E;*

(3) 95% of pieces have a modulus of rupture (*MOR*) greater than 2.1 times the assigned bending strength (F_b).

For MEL lumber:

(1) Average edge *MOE* equal to or greater than the assigned average *E;*

(2) 95% of pieces have edge *MOE* greater than 75% of assigned average *E;*

(3) 95% of pieces have a modulus of rupture (*MOR*) greater than 2.1 times the assigned F_b;

(4) 95% of pieces have an ultimate tensile strength greater than the assigned value.

From these quality control requirements, one can extract some information regarding the accuracy of SPIB-approved grading machines listed in Table 2.1 and work backwards to find the level of accuracy needed to meet the requirements in a feasible manner. A simulation of the grading process used these requirements to grade randomly generated samples; this is described in detail in Chapters 4 and 5.

2.3 Multiple Regression and Other Predictive Models

Multiple parameter regression models were first used in strength prediction by the same early pioneers in machine-grading (Muller 1968). Nearly all of the laboratories that first investigated the relationship between *R* and *E* also found that adding specific gravity, for instance, increased the correlation coefficient, though only modestly. Pearson (1965) found the correlation coefficients using green lumber of *R* and *E* and of *R* and modulus of rigidity (*G*) to be 0.85 and 0.84, respectively, but was improved to 0.94 when both *E* and *G* were included.

Ross and Pellerin (1988) predicted the bending strength of composite materials using density, stress wave velocity, and attenuation of stress waves. Divos and Tanaka (1997) predicted the bending strength of a mix of *Picea* and *Pinus* 2 x 4 lumber using the dynamic *E* in bending, concentrated knot diameter ratio, longitudinal dynamic *E*, screw withdrawal force, and *E* obtained from static bending tests. Many other studies have accurately predicted bending parameters using multiple regression with some combination of stresswave/vibrational measurements, knot

information and physical properties such as density (Garcia 2007; Wang et al. 2008; Divos and Kiss 2010; Vega et al. 2012). Esteban et al. (2009) predicted the static *E* from NDE measurements and applied an artificial neural network, which is analogous to multiple regression in that there are weights applied to various parameters for prediction.

2.4 Objectives

Currently in the literature, there is little research that deals with the building of predictive models of southern pine structural lumber in explicit context of the lumber grading process. There is much information on the development and application of nondestructive techniques and their use in multiple regression models dealing with the prediction of wood properties. However, southern pine is an uncommon specie in these studies which rarely go beyond the application of NDE techniques and development of a predictive model. This study demonstrates the application of nondestructive techniques to build predictive models for a commercially important specie but also deals with the feasibility of the models by simulating the grading process using the developed models. Since the machine-grading of southern pine is well-developed on an industrial scale, this study sought to develop novel approaches to model the strength and stiffness of lumber with nondestructive measurements. The developed visual parameters, as will be seen, may be significantly easier and faster to measure than those currently used and may be incorporated into current grading procedures.

The primary objective of this study is to accurately predict the mechanical properties commonly used as grading criteria – bending strength and stiffness – in southern pine 2x6 dimension lumber with a combination of nondestructive measurements and visual characteristics. Global measurements of board density, stress wave velocity and dynamic modulus of elasticity

along with local measurements of knots were used to predict the effect of these variables on global strength and stiffness of each board. The study consisted of several specific objectives:

1. Develop models to predict the bending properties of 2 in. x 6 in. x 8 ft. southern pine lumber using nondestructive physical measurements and visual observations.

2. Using the developed predictive models, simulate the lumber grading process adhering to the American Lumber Standards Committee Machine Graded Lumber Policy for machine evaluated lumber and following lumber grades in the Southern Pine Reference Design Values based on SPIB grading rules and the American Wood Council (AWC) National Design Specification®.

2.5 References

American Lumber Standards Committee, Inc. (ALSC). 1998. Machine graded lumber policy. Germantown, Maryland.

American Lumber Standards Committee, Inc. (ALSC). 2013. Grading machines approved by the board of review. Germantown, Maryland.

American Society for Testing and Materials (ASTM). 2007. Standard practice for establishing allowable properties for visually-graded dimension lumber from in-grade tests of full-size specimens. ASTM D1990-07. *In*: Annual Book of ASTM Standards. ASTM, West Conshohocken, Pennsylvania.

American Society for Testing and Materials (ASTM). 2011. Standard practice for establishing clear wood strength values. ASTM D2555-06(2011). *In*: Annual Book of ASTM Standards. ASTM, West Conshohocken, Pennsylvania.

American Society for Testing and Materials (ASTM). 2011. Standard practice for establishing structural grades and related allowable properties for visually graded lumber. ASTM D245-06. *In*: Annual Book of ASTM Standards. ASTM, West Conshohocken, Pennsylvania.

Bell, E. R., E. C. Peck, and N. T. Krueger.1950. Young's modulus of wood determined by a dynamic method. U.S. Forest Products Laboratory Report 1775. WI: U.S. Department of Agriculture, Forest Service, Forest Products Laboratory.

Divos, F. and F. S. Kiss. 2010. Strength grading of structural lumber by portable lumber grading -Effects of knots. *Conference COST Action E53 "The future of quality control for wood & wood products"*. Edinburgh, United Kingdom.

Divos, F. and T. Tanaka. 1997. Lumber strength estimation by multiple regression. *Holzforschung*. 51(5): 467-471.

Doyle, D. V. and L. J. Markwardt. 1966. Properties of southern pine in relation to strength grading of dimension lumber. US Forest Service Research Paper FPL-64. Madison, WI: U.S. Department of Agriculture, Forest Service, Forest Products Laboratory.

Esteban, L. J., F. G. Fernandez and P. de Palacios. 2009. MOE prediction in *Abies pinsapo* Boiss. timber: application of an artificial neural network using nondestructive testing. *Computers and Structures*. 87:1360-1365.

Forest Products Laboratory (FPL). 2010. Wood handbook – wood as an engineering material. General Technical Report FPL-GTR-190. Madsion, WI: U.S. Department of Agriculture, Forest Service, Forest Products Laboratory.

Fukada, E. 1950. The vibrational properties of wood. *Jour. Phys. Soc. Japan.* 5:321-7.

Galligan, W. L., and R. W. Courteau. 1965. Measurement of elasticity of lumber with longitudinal stress waves and the piezoelectric effect of wood. *Proc. of the 2nd Symp. on Nondestructive Testing of Wood*. Washington State Univ., Pullman, Wash.

Galligan, W. L. and K. A. McDonald. 2000. Machine grading of lumber—Practical concerns for lumber producers. Gen. Tech. Rep. FPL–GTR–7 (Revised). Madison, WI: U.S. Department of Agriculture, Forest Service, Forest Products Laboratory.

Garcia, M. C., J. I. F. G. Seco and E. H. Prieto. 2007. Improving the prediction of strength and rigidity of structural timber by combining ultrasound techniques with visual grading parameters. *Materiales de Construccion*. 57(288):49-59.

Gerhards, C. C. 1982. Longitudinal stress waves for lumber stress grading: factors affecting applications: state of the art. *For. Prod. J.* 32(2):20-25.

Glover, C. G. 1962. Statistical analysis of edge vs. flat modulus of elasticity data. Unpublished Report. Potlatch Forests, Inc. Lewiston, Idaho.

Hearmon, R. F. S. and J. N. Burcham. 1954. The dielectric properties of wood. Forest Prod. Res. Spec. Rep. 8. Dep. Sci. Ind. Res. London, United Kingdom.

Hoerber, G. F. 1962. A study of modulus of elasticity and modulus of rupture in Douglas-fir dimension lumber. Unpublished Report. Potlatch Forests, Inc. Lewiston, Idaho.

Hofstrand, A. D. and J. P. Howe. 1960. Comparison of modulus of elasticity and modulus of rupture in white fir dimension lumber. Consultants' Research Report No.2. Potlatch Forests, Inc. Lewiston, Idaho.

Ihlseng, M. C. 1878. The modulus of elasticity in some American woods, as determined by vibration. *Van Nostrand's Eng. Mag*. Vol. XIX 8-9.

Ihlseng, M. C. 1879. On a mode of measuring the velocity of sound in wood. *Am. J. of Sci*. Third Ser., XVII(98):125-132.

James, W. L. 1964. Vibration, static strength and elastic properties of clear Douglas-fir at various levels of moisture content. *Forest Prod. J*. 14(9):409-413.

Jayne, B. A. 1959. Vibrational properties of wood as indices of quality. *Forest Prod. J.* 9(11): 413-416.

Kitazawa, G. 1950. Nondestructive testing for forest products. *Proceedings: Forest Products Res.Soc*. 4:191-197.

Matsumoto, I. 1962 . Studies on the dynamic modulus E and logarithmic decrement of wood by transverse vibrations. *Bull. of the Kyushu University Forests*.36. Fukuoka, Japan.

Matthews, P. C. 1987. Wood, light and objective scanning. *In:* Proc. Of 2nd Inter. Conf. on Scanning Technology in Sawmilling. Miller Freeman Publications, San Francisco, California.

McDonald, K. A. and B. A. Bendtsen 1986. Measuring localized slope of grain by electrical capacitance. *Forest Prod. J*. 36(10):75-78.

McLauchlan, T. A., J. A. Norton and D. J. Kusec. 1973. Slope-of-grain indicator. *Forest Prod. J.* 23(5): 50-55.

Muller, P. H. 1968. Mechanical stress-grading of structural timber in Europe, North America and Australia with a research programme on this field for South Africa. *Wood Sci Tech.* 2(1):43-72.

Norimoto, M. and T. Yamada. 1972. The dielectric properties of wood. VI. On the dielectric properties of the chemical constituents of wood and the dielectric anisotropy of wood. *Wood Res*. 52:31-43.

Pearson, R. G. 1965. The Establishment of Working Stresses for Groups of Species. Technological Paper 17 No. 35. Division of Forest Products, Australian CSIRO.

Pellerin, R. F. 1965. A vibrational approach to nondestructive testing of structural lumber. *Forest Prod. J*. 15(3):93-101.

Peterson, R. W. 1960. The dielectric properties of wood. FPL Tech. Note 16. Canada Forest Products Laboratory. Ottawa, Canada.

Rajeshwar, B., D. A. Bender, D. E. Bray and K. A. McDonald. 1997. An ultrasonic technique for predicting tensile strength of southern pine lumber. *Transactions of the ASAE*. 40(4): 1153-1159.

Ross, R. J. and R. F. Pellerin. 1988. NDE of wood-based composites with longitudinal waves. *Forest Prod. J.* 38(5):39-45.

Ross, R. J. and R. F. Pellerin. 1994. Nondestructive testing for assessing wood members in structures: A review. Gen. Tech. Rep. FPL-GTR-70 (Rev.). Madison, WI: U.S. Department of Agriculture, Forest Service, Forest Products Laboratory.

Sandoz, J. L. 1989. Grading of construction timber by ultrasound. *Wood Sci. Technol.* 23(1):95-108.

Soest, J. F.1987. Laser scanning technique for defect detection. *In:* Proc. Of 2nd Inter. Conf. on Scanning Technology in Sawmilling. Miller Freeman Publications, San Francisco, California.

Southern Pine Inspection Bureau (SPIB). 2002. Standard grading rules for southern pine lumber. Pensacola, Florida.

Vega, A., A. Dieste, M. Guaita, J. Majada and V. Bano. 2012. Modelling of the mechanical properties of *Castanea sativa* Mill. structural timber by a combination of non-destructive variables and visual grading parameters. *Eur. J. Wood Prod.* 70(6):839-844.

Wang, S. Y., J. H. Chen, M. J. Tsai, C. J. Lin and T. H. Yang. 2008. Grading of softwood lumber using non-destructive techniques. *J. Mat. Proc. Technol.*208(1-3): 149-158.

Yavorski, J. M. 1951. A review of electrical properties of wood. Tech. Publication 73. State Univ. N.Y., Coll. Forest. Syracuse, New York.

3. MATERIALS AND METHODS

3.1 Materials

Materials for this study consisted of two independent sets of kiln-dried 2x6 southern pine boards eight feet in length (1.5 in. x 5.5 in. x 96 in.). The training set of 89 samples came from a Weyerhaeuser mill in Holden, Louisiana; these were used to develop the models which were later validated with a separate set. The exact grade of each of the samples was unknown, but the static modulus of elasticity (MOE_s) and modulus of rupture (MOR) were normally distributed over a wide range of values and most likely contained boards from the highest visual grade, Select Structural, to the lowest grade, No. 3 and Stud. Several boards were of poor quality and many contained blue stain, noticeable compression wood and/or extreme warp that would severely limit its grade (Figure 3.1). Another 60 kiln-dried samples used for model validation came from a separate Weyerhaeuser mill in McComb, Mississippi. Both sets were conditioned indoors at room temperature (65 % relative humidity and 70 ^{o}C) for at least a week prior to testing.

The moisture content of each board was calculated after static bending tests according to ASTM D4442 (2003). A small sample near the location of failure was removed, weighed immediately following the test, oven-dried and then weighed again. The average moisture content for all of the boards was about 15%. Density (ρ) was calculated from the weight and volume of each sample. Each board was weighed using an electronic balance and volume was held constant for each board and assumed to be identical in dimension – 5.5 in. x 1.5 in. x 96 in. Missing wood due to wane was considered negligible and therefore ignored. The average density for the training set was 35.26 lb./ft^3, or a specific gravity of 0.565; average density for the validation set was 33.9 lb./ft^3, or a specific gravity of 0.543.

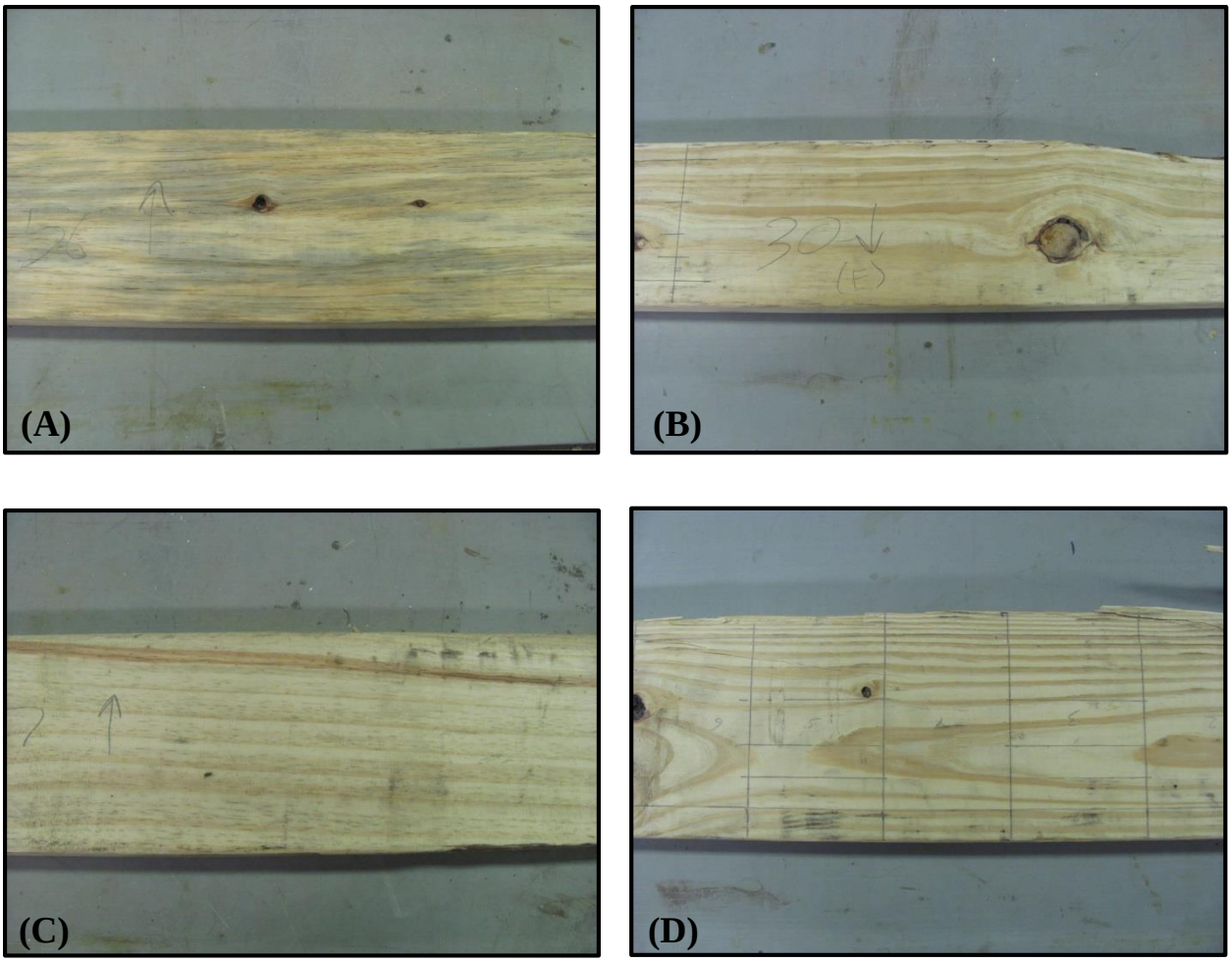

Figure 3.1 – Samples illustrating range of board quality; (A) sample with heavy blue stain, (B) and (C) samples with compression wood, (D) high quality sample with neither stain nor compression wood

3.2 Experimental Methods

The predictive models developed in this study utilized several nondestructive and visual variables which are separated into two categories: global and local measurements. Global parameters measure a particular property of the entire board, whereas local parameters measure the visual characteristics of a particular region of the board. The global measurements function as a base from which penalties of local defects can be made. First, it is important to be reminded of the basic mechanics of a beam in bending to understand the motivation for the localized, visual parameters used in this study.

The stress distribution in a beam in third-point bending varies along the longitudinal distance and across the cross section (Figures 3.2 and 3.3). In the case of a simple beam with two equal concentrated loads symmetrically placed, the maximum moment occurs between the loads, or the inner-third of the span (Figure 3.3). The moment changes linearly between the maximum moment at the inner-third and the reaction points, where there is zero moment.

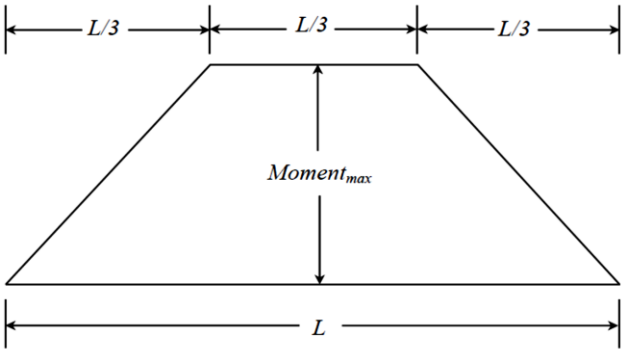

Figure 3.2 – Distribution of bending stress in beam during static, third-point bending

Similarly, the axial force acting on the cross-section of the beam also behaves in a linear fashion (Figure 3.3). The maximum compressive and tensile force occur at the upper and lower edge, respectively, and decrease linearly to zero at the neutral axis.

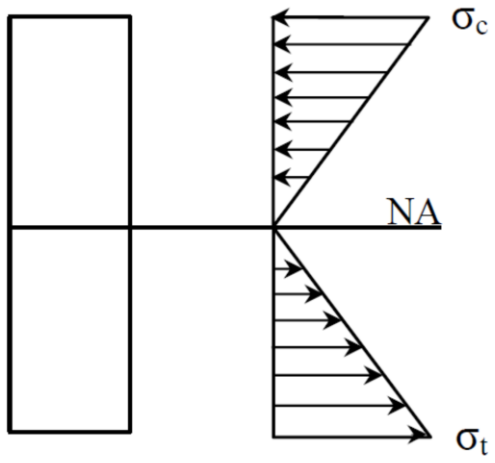

Figure 3.3 – Distribution of cross-sectional axial stress in beam during static, third-point bending

Since the axial stress distribution and bending moment can be approximated by simple linear relationships, it is relatively straightforward to estimate the effect of knots based on the location. There is much literature on the detrimental effect of knots on the mechanical properties of lumber (Kunesh and Johnson 1972; Phillips et al. 1981; Bodig and Jayne 1982; Nguedjio 1999); however, Corder (1965) was one of the first of many to notice that isolated knots may cause a local depression in the stiffness profile measured along the length of a flat-wise member by a grading machine. Therefore, it seemed intuitive to create a grid-like structure upon each sample to account for the general location of the defect along the length and depth of the member. Knots that are located on the edge of a board, particularly in tension, have a much more significant effect on bending strength than knots of equal size near the neutral axis, which has zero stress. Each grid, with its location specific information, may be treated as a variable which may be 'turned on' if a defect is present.

A rectangular grid was drawn on the wide surface of each sample dividing the board into 112 rectangular sections (Fig. 3.4). The grid spans 48 in. across the middle portion, centered at the mid-span of the sample, and consists of 16 three-inch long rectangles. The first three rows from the edges were each approximately ¾ in. wide and the middle row was one in. wide.

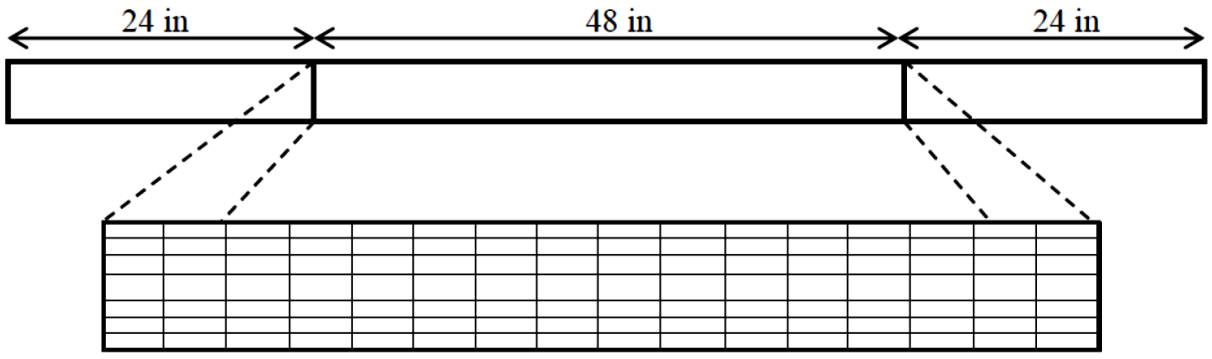

Figure 3.4 – Grid arrangement on inner-half (48 in) of the sample. The three outer rows are each ¾ in wide and inner row is 1 in. wide; all grids are 3 in. in length

3.2.1 Global Parameters

Several physical and mechanical properties related to bending strength and stiffness were measured for each sample (Table 3.1). Global parameters do not necessarily account for small, localized variations such as slope of grain and knots but are still significant factors for predicting mechanical properties, even for full-size structural lumber.

Table 3.1 – Physical and mechanical global parameters

Variable	Definition
ρ	Density (lb./ft^3)
V_{ave}	Average ultrasonic wave velocity (ft./s)
V_{min}	Minimum ultrasonic wave velocity (ft./s)
MOE_d	Ultrasonic dynamic modulus of elasticity (lb./in^2)

Average and minimum stress wave transmission velocity, V_{ave} and V_{min} , were measured for each sample using a handheld acoustic meter and a hammer (Director HM200, Fibre-gen) prior to static bending tests. Each board was held at one end by a rubber stopper on a table and the acoustic receiver was pressed against the free end of the board. The sound wave produced by the hammer at the free end travelled through the board, reflected off the stopper at the other end and travelled back through the board where it was received by the meter. The stress wave velocity was recorded four times across the free end of each board and the dynamic modulus of elasticity (MOE_d) was calculated by:

$$MOE_d = \rho V^2 \tag{3.1}$$

where ρ = density of the sample and V = wave transmission velocity

The static modulus of elasticity (MOE_s) was obtained from a third-point bending test in accordance with ASTM D198 (2009) with a Riehle testing machine. The span was set to seven ft. and loading rate was calculated to obtain maximum load in no less than six minutes and no greater

than 20 minutes. A brace was placed between each load point and reaction point in order to resist lateral deflection. Maximum load, modulus of rupture and static *E* were automatically calculated by data collection software and verified with manual calculations.

3.2.2 Visual Parameters

Several knot and ring measurements were used as visual variables in the analysis (Table 3.2). The average rate of growth was measured at each end of the sample according to Section 103 of the Southern Pine Inspection Bureau's *Standard Grading Rules of Southern Pine Lumber* (SPIB 2002). The annual rings per inch were measured on a "representative radial line" over a continuous length of 3 in. or as nearly 3 in. as is available. The variables $Ring_{min}$ and $Ring_{ave}$ are the minimum and average annual rings per inch for the two ends of each sample, respectively.

Table 3.2 – Visual variables used in analysis

Variable	Definition
$Ring_{min}$	Minimum rings/inch on either end of board
$Ring_{ave}$	Average rings/inch of both ends of board
$\sum Row_i$	Sum of cells containing defects in row *i*
$\sum Column_j$	Sum of cells containing defects in column *j*

All visible knots and defects were recorded for each sample using the grid system (Figure 3.4). For each of the two or three visible faces of a particular cell, a value of '1' was assigned if it contained a knot greater than ¼ inch in either dimension and assigned a '0' if the cell face is free of defects (Table 3.3). Each cell has at least two visible sides; the outer edge cells containing the top and bottom (compression and tension) faces have three (Figure 3.5). Knots that are completely contained within a cell that are less than ¼ inch were not recorded as their effect on mechanical properties is minimal, considering both the reduction in cross section and the slope of grain due to knots. The portion of a knot that crosses a cell boundary that is less than ¼ in. is not recorded as a

defect. Cracks, splits, wane, pith and other defects, though they undoubtedly affect mechanical properties, were ignored in this study. These were considered too difficult to measure and most likely insignificant compared to the effects of knots.

Table 3.3 – Value assigned to individual cells based on defects

Individual Cell Score	Interpretation
0	No defects present on any face
1	Defect on one face
2	Defect on two faces
3	Defect on each visible face (only applicable to cells on outer edges with three visible sides)

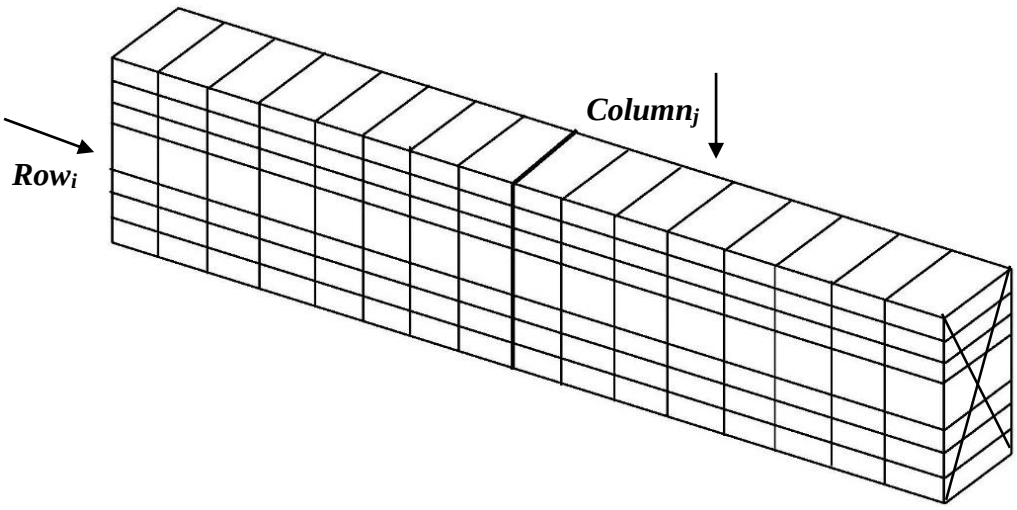

Figure 3.5 – Three-dimensional schematic of inner-third of sample with grid system; cells contain two or three faces depending on the row

The summation variables, Σ Rowi and Σ Columnj , were created to account for both the location and amount of defects for every section of the sample. Rowsi (i = 1, 2, …, 7) represent the sections of cells oriented longitudinally along the board and Columnsj (j = 1, 2, …, 8) represent the sections of cells oriented along the width (Figure 3.5). Row1 corresponds to the first row of cells from the top of the sample, Row2 with the second, and so on. Row4 is the central row and contains the neutral axis. Column1 is the first column from the center of the board and Column8

is the column furthest from the center of the board. Although there are two sets, one for each side of the sample, this is not consequential since $Column_j$ variables were not used in the analysis. To calculate $\Sigma\, Row_i$, the total number of cells containing defects are summed for each face of each cell in Row_i. Similarly, $\Sigma\, Column_j$ is calculated by summing the total number of cells containing defects for each face of each cell in column j. In other words, the individual cell scores from Table 3.3 were summed for cells in the particular row and column.

3.3 Statistical Analysis and Predictive Models

3.3.1 Model Training

Multiple linear regression models were constructed using the global physical parameters and visual parameters (Table 3.4). The multiple linear regression models take the form:

$$y_i = \beta_0 + \beta_1 x_{i1} + \beta_2 x_{i2} + \ldots + \beta_p x_{ip} + \varepsilon_i \quad \text{for } i = 1, 2, \ldots \tag{3.3}$$

where β_0 is the intercept, β_p are the parameter coefficients, x_{ip} is the j^{th} predictor variable for the i^{th} observation and ε_i is the residual error if the i^{th} observation.

From all the possible models that included all combinations of variables, models were selected based on several criteria: goodness of fit, predictive performance, and simplicity. One model may be superior to another for fitting the original training set of data, yet may perform worse during validation of the new set of samples. Ultimately, the simplest model with best predictive performance was chosen.

Based upon initial results of the relationship between dynamic modulus of elasticity, MOE_d, calculated from average wavespeed and density (Equation 3.1) and the static modulus of elasticity, MOE_s, several outliers that significantly altered the model were identified (Figure 3.6). The linear regression model predicting MOE_s from MOE_d was significantly improved when these samples were removed. As it turns out, these samples have characteristics that justify their removal

from the regression. Nevertheless, two sets of models were created: models that include these abnormal samples and models that remove them from the analysis. As will be explained in Chapter 4 and Chapter 5, models that do not include these influential samples were preferred.

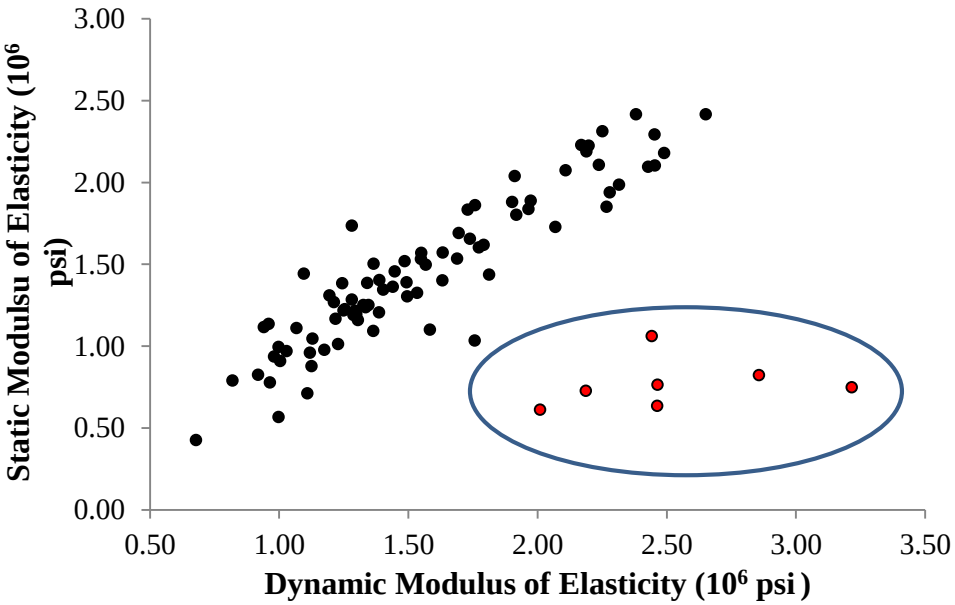

Figure 3.6 – Scatterplot of dynamic modulus of elasticity and static modulus of elasticity; circled points indicate samples that do not follow general relationship

3.3.2 Model Validation and Tuning

The independent set of 60 samples obtained from a Weyerhaeuser mill in McComb, Mississippi were used to validate the models created from the training set. Physical and visual measurements specified in the model were measured for each sample and the mechanical properties were predicted using the training model. The testing procedure for static bending, moisture content, and density/specific gravity was identical to that described for the training set. Samples from the validation set contained boards of various visual grades – 20 samples each of No. 1, No. 2 and No.3 – unlike the training set which was a mixture of un-graded samples.

Based on the performance of each model using the validation set, as measured by the standardized sum of squared error, one of the models was chosen. To further improve the model,

the training set and validation set were combined and regression was performed again to tune the parameter estimates and develop the final models used for the simulation study. This final stage of combining and tuning was not done for models that contained all samples, only those that had the influential samples removed.

3.4 Grading Simulation and Optimization

The distribution of predicted MOE_s, *MOR* and model residuals were estimated using goodness of fit tests from the combined training and validation sets. Based on the estimated distribution parameters, 5,000 random numbers were generated from the distribution for the predicted MOE_s and *MOR* calculated from the final, tuned regression models. Since the residuals are normally distributed with equal variance, residuals were also generated for MOE_s and *MOR* and randomly added to each randomly generated "predicted" variable. The end result is 5,000 samples that have nearly identical distributions of the predictive variables, with nearly identical distribution of residuals.

Using the randomly generated numbers from the estimated distribution of MOE_s and *MOR*, a simulated grading study was performed to analyze the models' performance. Grade rules described by the American Lumber Standards Committee (ALCS) and Southern Pine Design Reference are followed to place simulated samples into already established grades in the AWC NDS®. Performance of the model will be checked by comparing the proportion of samples that do not meet minimum grade requirements.

3.5 References

American Society for Testing and Materials (ASTM). 2007. Standard test methods for direct moisture content measurement of wood and wood-base materials. ASTM D4442-07. *In*: Annual Book of ASTM Standards. ASTM, West Conshohocken, Pennsylvania.

American Society for Testing and Materials (ASTM). 2013. Standard test methods of static tests of lumber in structural sizes. ASTM D198-13. *In*: Annual Book of ASTM Standards. ASTM, West Conshohocken, Pennsylvania.

Bodig J. and B. A. Jayne. 1982. Mechanics of wood and wood composites. Van Nostrand Reinhold, New York.

Corder, S. E. 1965. Localized deflection related to bending strength of lumber. *In:* Proc. of the Second Symposium on Nondestructive Testing of Wood. Spokane, Washington.

Kunesh R. H. and J. W. Johnson. 1972. Effect of single knots on tensile strength of 2- by 8- inch Douglas-Fir dimensional lumber. *For. Prod. J.* 22(1): 32–37.

Nguedjio, C. F. 1999. Effect of knots on the relation between flatwise and edgewise stiffness. *In:* Proc. of PACIFIC timber engineering conference. Rotorua, New Zealand

Phillips G. E, J. Bodig and J. R. Goodman. 1981. Flow-grain analogy. *Wood Sci.* 14: 55–64

Southern Pine Inspection Bureau (SPIB). 2002. Standard grading rules for southern pine lumber. Pensacola, Florida.

4. RESULTS

4.1 Training Set, All Samples

All 89 samples in the training set were used in the analysis, which included the group of influential samples circled in Figure 3.6. The coefficient of determination (R^2) for each of the predictor variables and static modulus of elasticity (MOE_s) and modulus of rupture (MOR) were determined using ordinary least-squares regression (Table 4.1). Taken individually, each variable does not explain the behavior of either mechanical property particularly well. One point of interest is the relatively large R^2 between the ring variables and MOE_s – 0.558 and 0.530 for $Ring_{min}$ and $Ring_{ave}$, respectively. None of the column summation variables, $\Sigma\, Column_j$, yielded interpretable or significant results and are not included in any further analysis. Dynamic modulus of elasticity (MOE_d) and wavespeed variables of average wavespeed and minimum wavespeed (V_{ave} and V_{min}, respectively) appear to be slightly more useful in determining stiffness rather than strength, while the visual summation of knots variable, $\Sigma\, Row_i$, are better suited for explaining strength.

These results confirm the correlation between knots and reduction in mechanical properties as well as the effect of the location of knots in the cross section. This is done without directly measuring knot size or calculating time-consuming or complicated secondary knot measurements, such as the knot diameter ratio (Japanese Agricultural Standard 1991), concentrated knot diameter ratio (Divos and Tanaka 1997) or the knot depth ratio (Oh et al 2010). A very clear trend is evident that as the amount of knots in a longitudinal section (Row_i) increases and the distance from the neutral axis (Row_4) increases, the greater effect it has on the bending strength and, to a much lesser extent, stiffness. Knots in the tension section (Row_5, Row_6 and Row_7) account for more variation than those in the compression section (Row_1, Row_2 and Row_3) with the neutral axis having the minimum influence on both strength and stiffness. The advantage of removing influential samples

is already apparent; the correlation of every individual physical and visual variable except for the ring measurements increases. Dynamic *MOE,* for example, increases from 0.279 to 0.852 just by removing the seven influential samples.

Table 4.1 – Variables used in linear regression and coefficient of determination with MOE_s and *MOR* for training set using all samples and removing influential samples

	All Samples		Influential Samples Removed	
Variable	R^2 (MOE_s)	R^2 (*MOR*)	R^2 (MOE_s)	R^2 (*MOR*)
ρ	0.288	0.305	0.320	0.321
V_{ave}	0.183	0.139	0.741	0.245
V_{min}	0.265	0.187	0.716	0.251
MOE_{dyn}	0.279	0.252	0.852	0.391
$Ring_{min}$	0.558	0.213	0.506	0.235
$Ring_{ave}$	0.530	0.196	0.505	0.240
$\Sigma\, Row_i$	R^2 (MOE_s)	R^2 (*MOR*)	R^2 (MOE_s)	R^2 (*MOR*)
Row_1	0.086	0.141	0.114	0.199
Row_2	0.091	0.132	0.139	0.162
Row_3	0.051	0.110	0.084	0.137
Row_4	0.017	0.072	0.038	0.079
Row_5	0.046	0.169	0.087	0.178
Row_6	0.058	0.250	0.102	0.279
Row_7	0.097	0.291	0.112	0.324

4.1.1 Static Modulus of Elasticity Model

The optimal regression equation for predicted MOE_s, $PMOE_s$, includes just four parameters (Table 4.2). It can be written as:

$$PMOE_s = -872{,}371 + (169{,}237 \times Ring_{min}) + (24{,}444 \times \rho) + (54.1791 \times V_{min}) - (46{,}410 \times Row_7) \quad (4.1)$$

The ANOVA source table indicates that the model is highly significant (F value = 53.86, p <0.0001) with relatively high R^2 with just four parameters and an intercept term (Table 4.3). Several candidate models were considered but Equation 4.1 was considered the best model based on the selection criteria mentioned in Chapter 3.3.1. In addition to fitting the training set the best, Equation 4.1 had the lowest standardized sum of squared errors of all models for the validation set of samples, indicating better predictive performance.

Table 4.2 – Parameter estimates, standard error and t values for MOE_s model; training set, all samples

Variable	Parameter Estimate	Standard Error	t-value	Pr > |t|
Intercept	-872,371	313,736	-2.78	0.0067
$Ring_{min}$	169,237	21,373	7.92	<.0001
ρ	24,444	8,151	3.00	0.0036
V_{min}	54.17909	15.1652	3.57	0.0006
Row_7	-46,410	10,466	-4.43	<.0001

Table 4.3 – ANOVA source table for MOE_s model; training set, all samples

Source	DF	Sum of Squares ($x10^{13}$)	Mean Square ($x10^{13}$)	F Value	Pr > F
Model	4	1.451081	0.3627703	53.86	<.0001
Error	85	0.565762	0.0067353		
Corrected Total	88	2.016843			

A scatterplot of the predicted and actual MOE_s shows the improvement of adding visual measurements $Ring_{min}$ and Row_7 to the regression model (Figure 4.1). There is still considerable scatter around the mean line but the cluster of outliers in Figure 3.6 was eliminated. The regression assumption of normally distributed residuals with equal variance were met.

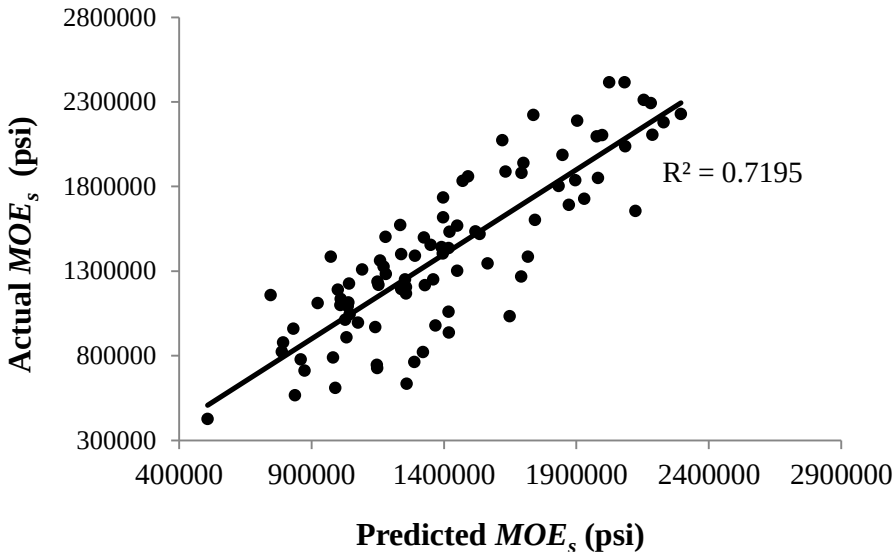

Figure 4.1 – Scatterplot of predicted and actual static modulus of elasticity using predicted MOE_s found by Equation 4.1

4.1.2 Modulus of Rupture Model

The optimal regression equation for predicted *MOR*, *PMOR*, uses five parameters (Table 4.4). The regression equation can be written as:

$$PMOR = -983 + (0.00228 \times PMOE_s) + (136.44 \times \rho) - (130.6 \times Row_1) - (307.3 \times Row_5) - (283.1 \times Row_7) \quad (4.2)$$

Table 4.4 – Parameter estimates, standard error and t values for *MOR* model; training set, all samples

Variable	Parameter Estimate	Standard Error	t Value	Pr > |t|
Intercept	-982.6	1539.5	-0.64	0.5251
$PMOE_s$	0.00228	0.0005356	4.26	<.0001
ρ	136.44	52.34	2.61	0.0108
Row_1	-130.6	64.67	-2.02	0.0467
Row_5	-307.3	104.03	-2.95	0.0041
Row_7	-283.1	65.16	-4.34	<.0001

The ANOVA source table indicates that the model is highly significant (F value = 39.96, p <0.0001) with relatively high R^2 with just five parameters and an intercept term (Table 4.5). The predicted MOE_s from Equation 4.1, $PMOE_s$, is used with density and three knot variables. A scatter plot of predicted *MOR* and actual *MOR* shows that the model is a reasonable fit to the data (Figure 4.2). As with predicted MOE_s, the regression assumptions were met.

Table 4.5 – ANOVA source table for *MOR* model; training set, all samples

	DF	Sum of Squares ($x10^8$)	Mean Square ($x10^7$)	F Value	Pr > F
Model	5	3.58551587	7.1710317	36.96	<.0001
Error	84	1.61023837	0.1940046		
Corrected Total	88	5.19575424			

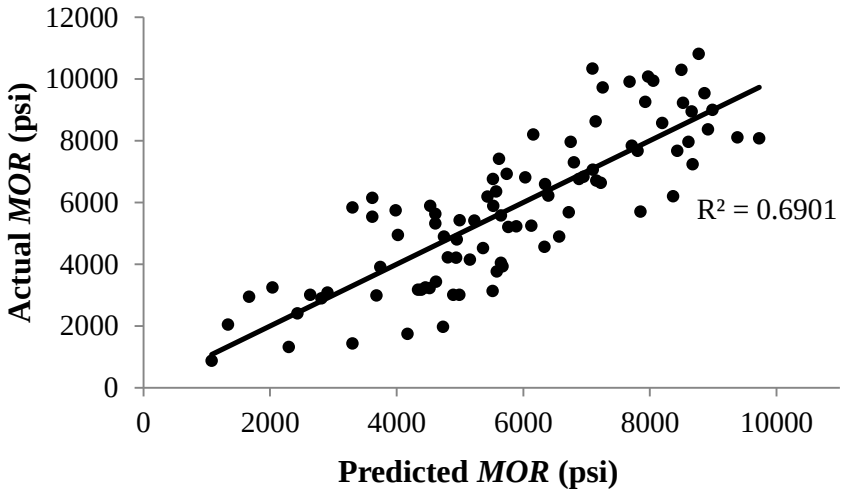

Figure 4.2 – Scatterplot of predicted and actual static modulus of rupture from Equation 4.2

4.2 Training Set, Influential Samples Removed

4.2.1 Static Modulus of Elasticity Model

Several outliers were removed from the analysis that significantly altered the regression. As can be seen in Figure 3.6, there is a group of samples that do not behave as the majority which

follow a linear trend. Diagnostic tests of individual data points such as Cook's Distance and studentized residuals confirm that these samples are outliers and significantly alter the regression using MOE_d as a predictor variable. Unless other variables are incorporated to account for these samples (as in the previous section), the only remedy is to remove them from the analysis. Since the MOE_s of the training set with all samples has a high coefficient of variation of 18.5%, some boards may need to be removed to meet the constraint of 15% for machine evaluated lumber suggested in the Wood Handbook (FPL 2010). These samples substantially increased the variability, and would most likely cause excessive variability within a grade. It was also especially difficult to predict their mechanical properties with stresswave techniques.

Another justification for removing these samples is a characteristic in the wavespeed measurements. There is an abnormality unique to only the removed samples: at least one of the four measured wavespeeds is greater than 18,000 ft./s. This is unique only to samples that are clear outliers; none that follow the general regression trend have measurements above 18,000 ft./s. This suggests that boards with abnormally high wavespeeds – in this case, greater than 18,000 ft./s – should not be included in standard predictive models for MOE_s or *MOR*. Other variables were combined to create a set of candidate models to compare (Table 4.6).

Table 4.6 – Candidate models for MOE_s model; training set, excluding samples with wavespeed greater than 18,000 ft./s

Variables in Model	R^2	Mean Square Error (x 10^{10})	Predicted Sum of Squares (x 10^{12})
MOE_d	0.8521	3.1347882322	2.63143
MOE_d , Row_7	0.8853	2.4627630763	2.179109
MOE_d, Row_7 , $Ring_{min}$	0.8923	2.3407282768	2.170981
V_{avg}, ρ, Row_7	0.8904	2.3830714384	2.128276
V_{avg} , ρ , Row_7 , $Ring_{avg}$	0.8994	2.2154581534	2.102773

There is little difference between most of the models built from the training set – comparable models were excluded from the table because of their similarity. However, the three-parameter model that includes average wavespeed, density and Row_7 was chosen because of its adequacy, predictive performance and its simplicity (Table 4.7 and Table 4.8, Figure 4.3). Of all candidate models, this model had the lowest standardized sum of squared errors in the validation set. One point of interest is that linear combinations of density and average wavespeed, the components used to calculate dynamic *MOE*, were better predictors of MOE_s than dynamic *MOE* itself. The regression equation can be written as:

$$MOE_s = -2{,}588{,}832 + (193.239 \times V_{avg}) + (39{,}086 \times \rho) - (33{,}502 \times Row_7) \quad (4.3)$$

Table 4.7 – Parameter estimates, standard errors and t-values for MOE_s model; training set, excluding samples with wavespeeds greater than 18,000 ft./s

Variable	DF	Parameter Estimate	Standard Error	t-value	Pr > |t|
Intercept	1	-2,588,832	186,437	-13.89	<.0001
V_{avg}	1	193.239	10.3978	18.58	<.0001
ρ	1	39,086	4,465	8.75	<.0001
Row_7	1	-33,502	6,526	-5.13	<.0001

Table 4.8 – ANOVA source table for MOE_s model; training set, excluding samples with wavespeeds greater than 18,000 ft/s

Source	DF	Sum of Squares ($x10^{13}$)	Mean Square ($x10^{12}$)	F Value	Pr > F
Model	3	1.509686	5.032285	211.17	<.0001
Error	78	0.185881	0.238308		
Corrected Total	81	1.695566			

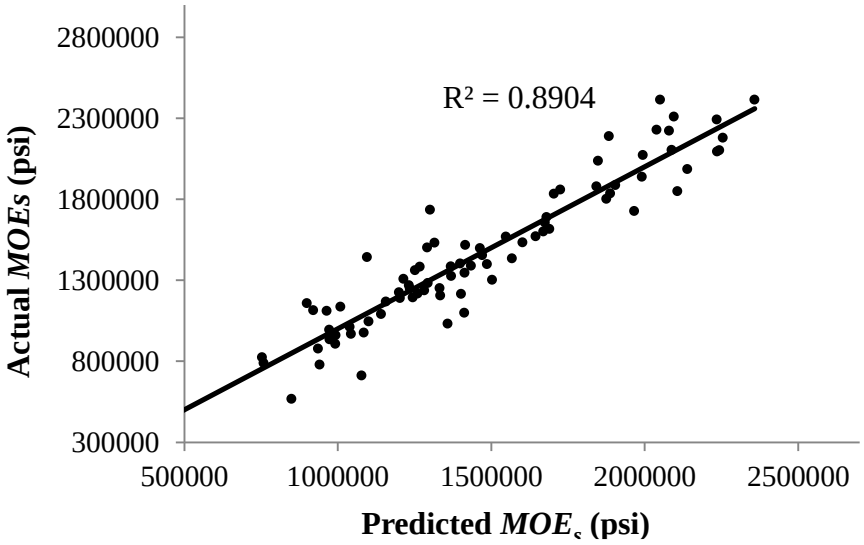

Figure 4.3 – Scatterplot of predicted MOE_s using Equation 4.3, training set excluding samples with wavespeeds greater than 18,000 ft./s

4.2.2 Modulus of Rupture Model

The predicted modulus of rupture (*PMOR*) was found by using the predicted MOE_s, $PMOE_s$, from Equation 4.3 or from combinations of density and average wavespeed. Several models are listed in Table 4.9 to illustrate the improvement when variables are added. There are hundreds of possible models, but most are practically the same or have multicollinearity problems (density, wavespeed, MOE_d, and *PMOE* are all highly correlated, for example). It is desirable to minimize the number of parameters in the model as this increases the predictive power and avoids over fitting the original sample set. As with the predicted MOE_s, the model with the best predictive performance as measured by smallest standardized sum of squared error in the validation set will be chosen. Ultimately, the five-parameter model was chosen which includes density and average wavespeed along with four row variables (Table 4.10 and 4.11, Figure 4.4). The regression equation is:

$$PMOR = -3{,}616 + (0.00262 \times PMOE_s) - (189 \times Row_1) - (266 \times Row_3) - (354 \times Row_6) - (190 \times Row_7) \quad (4.4)$$

Table 4.9 – Candidate models for *MOR* model; training set, excluding samples with wavespeed greater than 18,000 ft./s

Variables in Model	R^2	Mean Square Error ($x10^6$)	Predicted Sum of Squares ($x\ 10^8$)
$PMOE_s$	0.5013	3.085390	2.57198840
$PMOE_s$, Row_7	0.6165	2.402665	2.06698806
$PMOE_s$, Row_1 , Row_7	0.6619	2.145498	1.86503015
$PMOE_s$, Row_1 , Row_3, Row_6, Row_7	0.7121	1.874948	1.66602777
V_{avg} , ρ, Row_1 , Row_3, Row_6, Row_7	0.7442	1.688082	1.52083307

Table 4.10 – Parameter estimates, standard errors and t-values for *MOR* model; training set, excluding samples with wavespeeds greater than 18,000 ft./s

Variable	Parameter Estimate	Standard Error	t-value	Pr > |t|
Intercept	3,616	732	4.94	<.0001
MOE_s	0.00262	0.000402	6.51	<.0001
Row_1	-189	71.04	-2.66	0.0095
Row_3	-266	97.7	-2.73	0.0079
Row_6	-354	131.3	-2.69	0.0087
Row_7	-190	81.1	-2.34	0.0218

Table 4.11 – ANOVA source table for *MOR* model; training set, excluding samples with wavespeeds greater than 18,000 ft/s

Source	DF	Sum of Squares ($x10^8$)	Mean Square ($x10^7$)	F Value	Pr > F
Model	5	3.52426972	7.0485394	37.59	<.0001
Error	76	1.42496030	0.1874948		
Corrected Total	81	4.94923002			

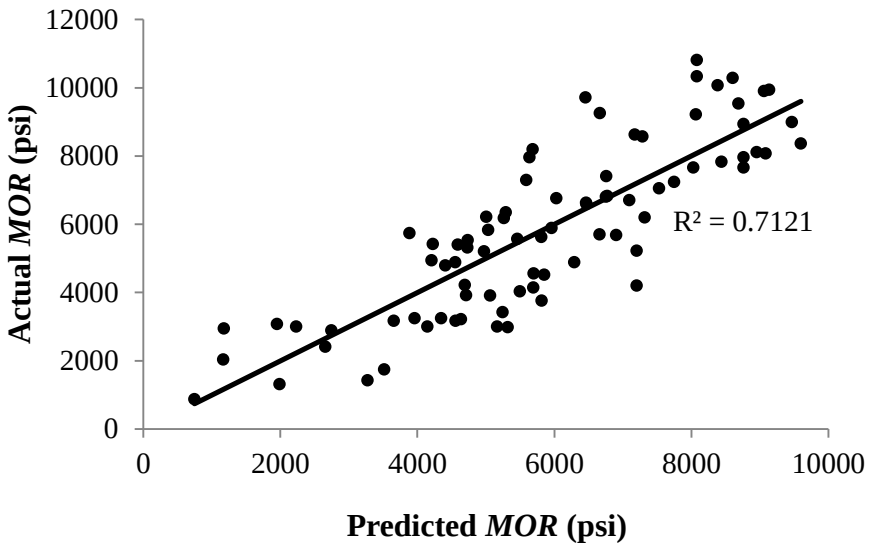

Figure 4.4 – Scatterplot of predicted *MOR* using Equation 4.4; training set excluding samples with wavespeeds greater than 18,000 ft./s

4.3 Validation of Models

Each candidate model for prediction of MOE_s and *MOR* using the training set was used with the validation set of 60 samples to assess the external predictive performance of each model. Generally the model with the lowest standardized sum of squared error in the validation set was chosen, provided regression assumptions and criteria were met. Both sets of models – excluding influential samples and including influential samples – performed reasonably well, but models that excluded influential samples performed better (Table 4.12, Figures 4.5 and 4.6). The drop in performance in the validation set for models that include all samples could be attributed to smaller sample size or, more likely, a smaller proportion of samples that are influential – seven out of 89 in the training set, but only two out of 60 in the validation set. The use of rate of growth measurements in models that include all samples could also be a problem as the method of measuring rings per inch is not precise. The "representative radial line" used to measure rate of growth is subjective and results vary widely with small changes in the line that is used.

Table 4.12 – Comparison of model performance of training and validation sets between models that include all samples and models with influential samples removed

	Model	Number of Samples	R^2 of Model
All Samples Included (Eq. 4.1 & 4.2)	Training MOE_s	89	0.7195
	Validation MOE_s	60	0.6276
	Training *MOR*	89	0.6901
	Validation *MOR*	60	0.6402
Influential Samples Removed (Eq. 4.3 & 4.4)	Training MOE_s	82	0.8904
	Validation MOE_s	58	0.8942
	Training *MOR*	82	0.7121
	Validation *MOR*	58	0.7184

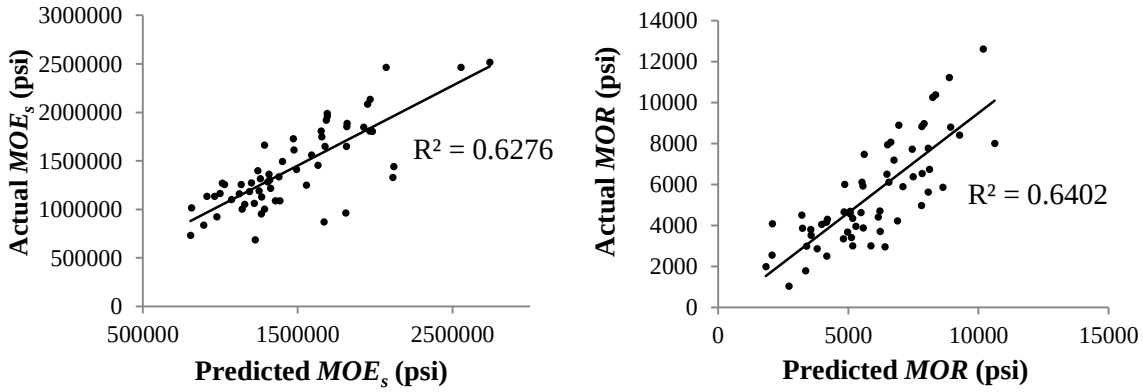

Figure 4.5 – Plots of predicted MOE_s and *MOR* using Equation 4.1 and 4.2, respectively, with validation set including all samples

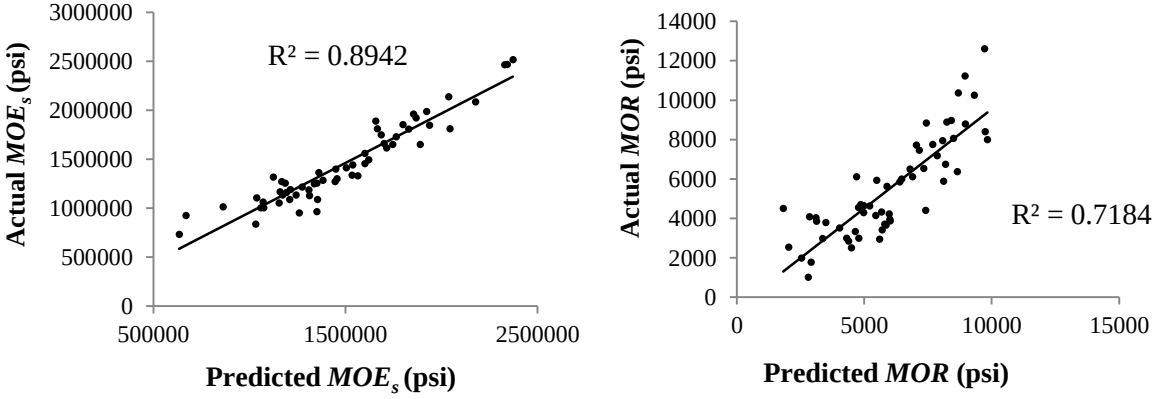

Figure 4.6 – Plots of predicted MOE_s and *MOR* using Equation 4.3 and 4.4, respectively, with validation set excluding samples with wavespeeds greater than 18,000 ft./s

4.4 Tuned Models, Combined Sets

Final models with tuned parameter estimates for both MOE_s and MOR were created by combining samples from the original training set with the validation set. After removing samples that had at least one wavespeed measurement greater than 18,000 ft./s, 140 remained in the analysis to tune the parameters. Models that included all samples were not tuned with combined sets since the removed boards would likely not be of sufficient quality for any machine grade. In an actual lumber grading process, if these inferior boards could be identified they would likely be removed from the grading process. If enough of these inferior samples could be obtained, new models could be specified that adequately fit all samples. The following models are the best predictive equations for MOE_s and MOR, provided that wavespeed restrictions are applied. The model parameters were largely unchanged from those found in the training set due to adequate fit in the validation set. As can be seen in Tables 4.13 through 4.16 and Figures 4.7 and 4.8, parameter estimates and regression models are highly significant. The characteristics of these models and the estimated distributions will be used in the grading simulation in the proceeding section.

4.4.1 Tuned Static Modulus of Elasticity Model

$$PMOE_s = -2{,}700{,}096 + (187.02 \times V_{avg}) + (44{,}307 \times \rho) - (31{,}870 \times Row_7) \quad (4.5)$$

Table 4.13 – Parameter estimates, standard errors and t-values for tuned MOE_s model; combined sets with samples removed

Variable	DF	Parameter Estimate	Standard Error	t value	Pr > |t|
Intercept	1	-2,700,096	142,106	-19.00	<.0001
V_{avg}	1	187.02	8.141	22.97	<.0001
ρ	1	44,307	3,521	12.59	<.0001
Row_7	1	-31,870	4,971	-6.41	<.0001

Table 4.14 – ANOVA source table for tuned MOE_s model; combined sets with samples removed

Source	DF	Sum of Squares ($x10^{13}$)	Mean Square ($x10^{12}$)	F Value	Pr > F
Model	3	2.398411	7.994703	373.61	<.0001
Error	136	0.291023	0.02139874		
Corrected Total	139	2.689434			

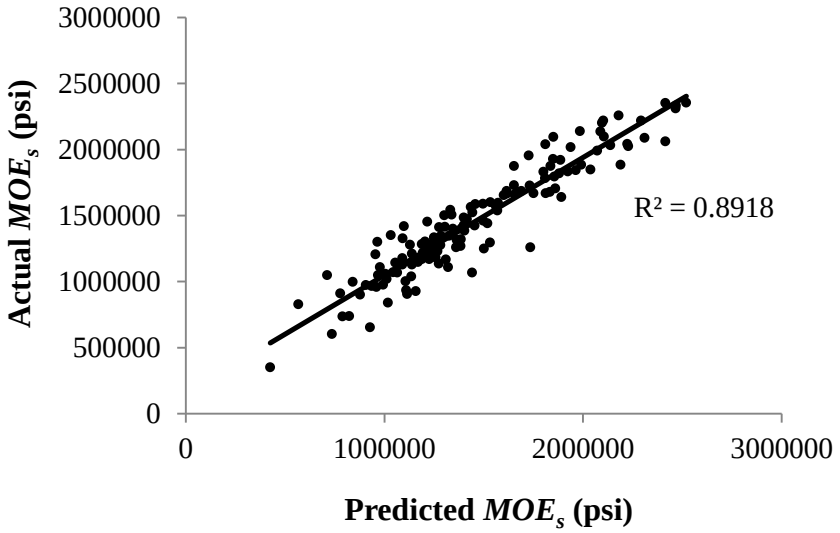

Figure 4.7 – Scatterplot of predicted MOE_s using Equation 4.5 and actual MOE_s for the combined sets

4.4.2 Tuned Modulus of Rupture Model

$$PMOR = 3{,}106 + 0.00281 \times (PMOE_s) - (183 \times Row_1) - (256 \times Row_3) - (352 \times Row_6) - (162 \times Row_7) \quad (4.6)$$

Table 4.15 – ANOVA source table for tuned *MOR* model; combined sets with samples removed

	DF	Sum of Squares ($x10^8$)	Mean Square ($x10^7$)	F Value	Pr > F
Model	5	6.17281676	12.3456335	66.75	<.0001
Error	134	2.47850916	0.1849634		
Corrected Total	139	8.65132592			

Table 4.16 – Parameter estimates, standard errors and t-values for tuned *MOR* model; combined sets with samples removed

Variable	Parameter Estimate	Standard Error	t Value	Pr > |t|
Intercept	3,106	606	5.12	<.0001
$PMOE_s$	0.00281	0.0003338	8.42	<.0001
Row_1	-183	58.2	-3.15	0.0020
Row_3	-256	70.8	-3.65	0.0004
Row_6	-352	103.6	-3.40	0.0009
Row_7	-162	66.2	-2.44	0.0159

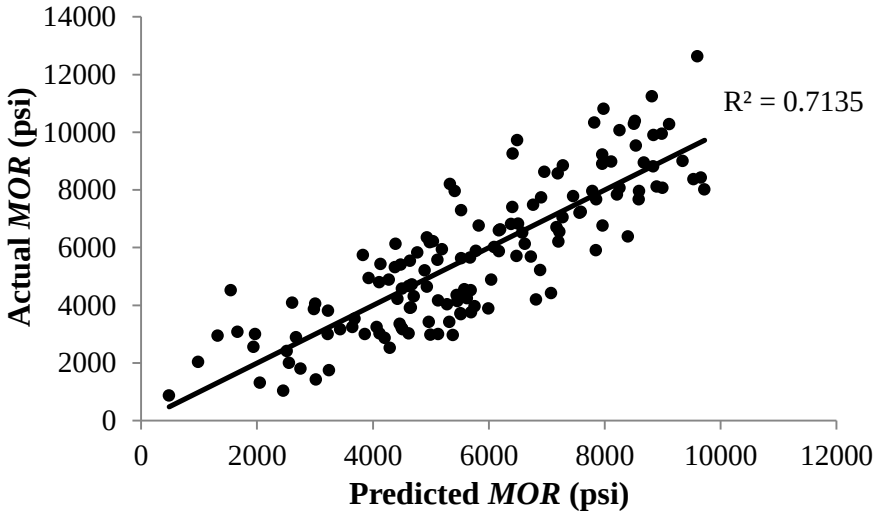

Figure 4.8 – Scatterplot of predicted *MOR* using Equation 4.6 and actual *MOR* for the combined sets

4.5 Grading Simulation Using Predictive Models

The estimated distribution parameters of predicted MOE_s and the standard deviation of the residuals from the combined set in Chapter 4.4 were used to generate 5,000 random samples. The primary purpose of the simulation is to have enough samples that have an equivalent distribution as the actual samples to provide a sufficient number to assess the performance of the predictive models for MOE_s and *MOR* across the entire range of values (Figure 4.9). The distribution of MOE_s, *MOR* and the residuals for both were found using PROC UNIVARIATE in SAS. Goodness

of fit tests yield p-values greater than the cutoff value of 0.05 for each test, thus failing to reject the null hypothesis that the variables follow the specified distribution (Table 4.17).

Table 4.17 – Distribution parameter estimates of predicted variables and residuals and accompanying tests

Variable	Distribution	Distribution Parameters		Test	P value
Predicted MOE_s	Lognormal	Mean: 1,457,760	St. Dev.: 459534	Kolmogorov-Smirnov	>0.150
Predicted MOE_s Residuals	Normal	Mean: 0	St. Dev.: 144,696	Shapiro-Wilk	0.1816
Predicted *MOR*	Weibull	Shape: 3	Scale: 6,397	Cramer-von Mises	>0.250
Predicted *MOR* Residuals	Normal	Mean: 0	St. Dev.: 1,335	Shapiro-Wilk	0.0580

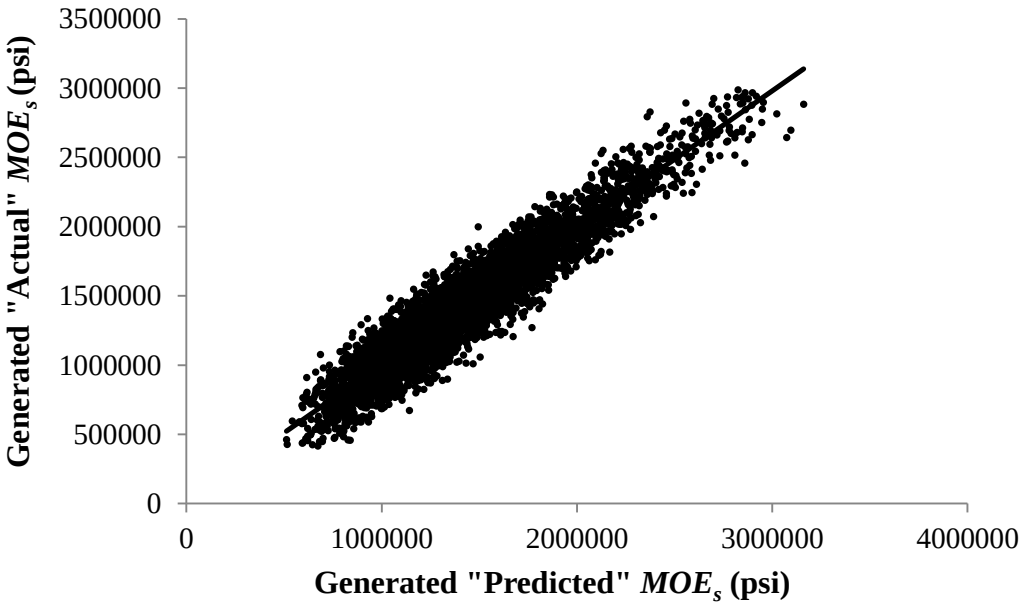

Figure 4.9 – Scatterplot of randomly generated "predicted" MOE_s and "actual" MOE_s using the distribution parameter estimates listed in Table 4.17

Predicted MOE_s follows a lognormal distribution and the prediction model (Equation 4.6) has normally distributed, homogeneous errors. Of the 5,000 randomly generated samples, values of "actual" MOE_s greater than 3.0 x 10^6 psi and less than 0.4 x 10^6 psi were removed as they were assumed to be unreasonable values for stiffness, which only resulted in 43 samples removed. In the original 140 samples which the distribution is derived from, the highest and lowest values for predicted MOE_s are 2,519,275 psi and 426,235 psi, respectively.

As mentioned in Chapters 2 and 3, each machine evaluated lumber (MEL) grade consists of an average modulus of elasticity, E, and an E_{min} value (defined as 75% of the assigned average E plus a 1.66 factor of safety). In order to simulate the grading process and match the average modulus of elasticity grades according to the NDS® for machine-evaluated southern pine lumber, intervals of the predicted MOE_s must be found such that the average value of actual MOE_s within the interval is equal to the grade. This is achieved by first calculating the average value of the probability density function (pdf), which in this case is lognormal with parameters listed in Table 4.17. The average value, y^*, on an interval [a, b] of a lognormal probability density function can be calculated with the following integral:

$$y^* = \frac{1}{b-a}\int_a^b \frac{1}{x\sigma\sqrt{2\pi}}\exp[-\frac{(\ln(x)-\mu)^2}{2\sigma^2}]dx \tag{4.7}$$

where a is the lower bound and b is the upper bound of the interval, μ is the mean and σ is the standard deviation of the distribution.

Solving equation 4.7, the average value, y^*, of the lognormal distribution is then:

$$y^* = \frac{\sigma^2\exp(\frac{\mu^2}{2\sigma^2})}{(b-a)(\mu-1)\sqrt{2\pi\sigma}}\left[\exp(ln(b)(\tfrac{\mu-1}{\sigma^2})) - \exp(ln(a)(\tfrac{\mu-1}{\sigma^2}))\right] \tag{4.8}$$

Equation 4.8 is the average value of the probability density function on interval [*a*, *b*]. To obtain *x*, the value of predicted MOE_s within the interval [*a*, *b*] that solves for y^*, the inverse of the probability density function must be solved. Using y^*, this becomes:

$$x = \exp[\frac{-2\sigma^2 \ln(y^*\sqrt{2\pi\sigma}) + \mu^2}{2(\sigma^2 - 2\mu + 1)}] \tag{4.9}$$

For any given distribution, the average value of predicted MOE_s can be found for any interval by a similar procedure of finding the average value of the pdf then calculating the inverse. However, since the actual MOE_s is of interest rather than the predicted MOE_s, an adjustment must be made to the interval bounds. A simple linear regression upon the generated "predicted" MOE_s and the "actual" MOE_s reveals the relationship of predicted MOE_s and the actual MOE_s as:

$$MOE_s = 0.9888x(PMOE_s) + 15,244 \tag{4.10}$$

First, the bounds of the probability density function of predicted MOE_s must be found such that the average value is equal to the value of interest, the actual MOE_s. By rearranging Equation 4.10, the bounds of predicted MOE_s needed to produce an average value of actual MOE_s are found by:

$$PMOE_s = \frac{MOE_s - 15,244}{0.9888} \tag{4.11}$$

Upper and lower bounds of "predicted" MOE_s were found to produce average values of "actual" MOE_s equal to the MEL grades between 1.0 x 10^6 psi and 2.2 x 10^6 psi in increments of 100,000 psi (Table 4.18). As can be seen from the table, the intervals are roughly 100,000 for each grade interval but vary slightly. The second requirement of 95% of samples within a grade having MOE_s greater than or equal to 75% of the assigned average *E* is met along with the first requirement of average *E* (Table 4.19). This E_{min} requirement is primarily related to the predictive ability of the model, or how variable the predictions are. However, this procedure is not as straightforward as finding the average value within a grade; details of this criteria will be discussed in Chapter 5.

Table 4.18 – Bounds for predicted average MOE_s required to produce average "actual" MOE_s, found by using Equations 4.7 through 4.11 for the specified distribution parameters

Average MOE_s (E grade-level)	"Predicted" *MOEs*			"Actual" *MOEs*		
	Bounds		Average MOE_s	Bounds		Average MOE_s
	Lower	Upper		Lower	Upper	
1,000,000	945,344	1,048,498	996,126	950,000	1,051,999	1,000,213
1,100,000	1,048,499	1,147,608	1,097,413	1,052,000	1,149,999	1,100,366
1,200,000	1,147,609	1,250,764	1,198,562	1,150,000	1,251,999	1,200,382
1,300,000	1,250,765	1,349,874	1,299,816	1,252,000	1,349,999	1,300,502
1,400,000	1,349,875	1,453,029	1,400,956	1,350,000	1,451,999	1,400,509
1,500,000	1,453,030	1,552,139	1,502,187	1,452,000	1,549,999	1,500,607
1,600,000	1,552,140	1,655,294	1,603,322	1,550,000	1,651,999	1,600,609
1,700,000	1,655,295	1,754,404	1,704,538	1,652,000	1,749,999	1,700,692
1,800,000	1,754,405	1,857,560	1,805,671	1,750,000	1,851,999	1,800,691
1,900,000	1,857,561	1,956,670	1,906,876	1,852,000	1,949,999	1,900,763
2,000,000	1,956,671	2,059,825	2,008,007	1,950,000	2,051,999	2,000,762
2,100,000	2,059,826	2,158,935	2,109,204	2,052,000	2,149,999	2,100,825
2,200,000	2,158,936	2,262,090	2,210,335	2,150,000	2,251,999	2,200,823

Table 4.19 – Summary of grades when sorted according to bin ranges in Table 4.18; samples are the randomly generated "actual" MOE_s values following distribution parameters in Table 4.17

Grade Bin Average E	Samples in Bin	Sample Mean MOE_s	Sample Standard Deviation	Proportion below 75% Average E
1,000,000	359	1,000,925	145,230	0.031
1,100,000	428	1,101,122	143,981	0.040
1,200,000	486	1,199,757	153,232	0.029
1,300,000	514	1,292,737	150,752	0.014
1,400,000	466	1,403,694	145,234	0.006
1,500,000	432	1,495,545	141,313	0.005
1,600,000	366	1,609,059	143,820	0.000
1,700,000	310	1,705,103	151,545	0.003
1,800,000	246	1,789,633	151,480	0.004
1,900,000	198	1,916,885	137,287	0.000
2,000,000	156	1,982,666	129,591	0.000
2,100,000	113	2,111,945	167,236	0.000
2,200,000	99	2,192,352	151,881	0.000

Predicted *MOR* follows a Weibull distribution with normally distributed, homogeneous residuals. To generate the random samples, the same procedure was followed as for the MOE_s simulation. Using the Weibull distribution parameters listed in Table 4.17 for predicted *MOR*, 5,000 random numbers were generated to create "predicted" values of *MOR*. Another 5,000 random numbers were generated from a normal distribution with parameters identical to *MOR* residuals and these numbers were added to the "predicted" *MOR* to create "actual" values of *MOR* (Figure 4.10). Samples that had final values of 400 or less were removed from the analysis as these were considered unrealistic values of *MOR* (the lowest value from both the combined sets was 870 psi); only 67 generated numbers were omitted.

For machine-evaluated lumber, 95% of the pieces within a grade must have a *MOR* greater than 2.1 the assigned bending stress, F_b. Since there is no specification for average *MOR*, the sorting process is slightly different than with MOE_s. Unlike the MOE_s grading process, a range of predicted values does not need to be specified to produce an average value for the grade. Only a minimum value of F_b is specified, which is really nothing more than the lower bound of the prediction limit for the value of predicted *MOR* found from regression, divided by 2.1 for the factor of safety. Given a prediction model, for any level of predicted *MOR* – the predicted value from Equation 4.6 – a lower 95% prediction interval can be calculated to ensure that 95% of future samples have actual *MOR* above this value. The assigned bending stress at a given level of predicted *MOR*, $F_{b|i}$, can be calculated by:

$$F_{b|i} = \frac{\widehat{Y}_i - 1.645\widehat{\sigma}\sqrt{x_i'(X'X)^{-1}x_i}}{2.1} \tag{4.11}$$

where Y_i is the predicted *MOR* at the i^{th} level, x_i are the covariates for the sample and X is the matrix of observations.

Since each level of predicted *MOR* ensures that 95% of samples at this specified level will be above $F_{b|i}$, each level of predicted *MOR* (or its prediction interval) could constitute a grade. Instead, common practice is to define narrow intervals of 50, 100 and 150 psi to sort samples based on *MOR*. In practice, a sample that has a calculated $F_{b|i}$ greater than or equal to that specified in a grade and less than the next highest value should be placed in that grade. For example, the M-32 MEL grade has an assigned F_b of 750 psi while the next highest grade, M-33, has an assigned F_b of 850 psi. Samples that have an estimated $F_{b|i}$ calculated from Equation 4.11 greater than or equal to 750 psi and less than 850 psi should be placed into M-33, assuming the *E* criteria is met.

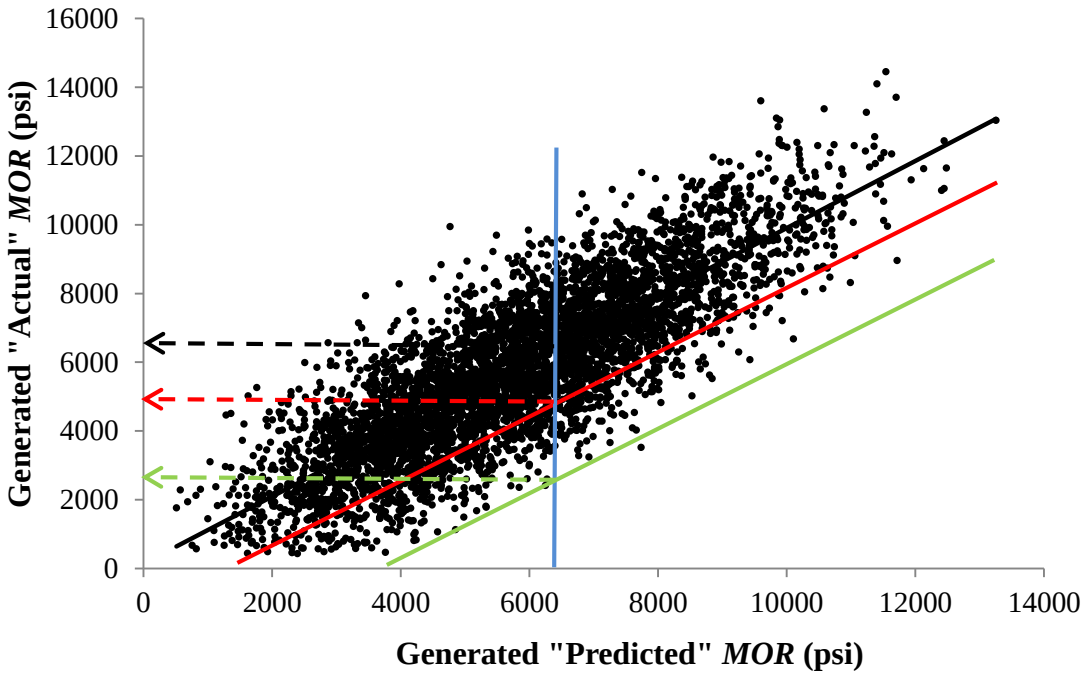

Figure 4.10 – Scatterplot of generated "predicted" *MOR* and "actual" *MOR* from parameter estimates in Table 4.17; for a given level of predicted *MOR* (blue vertical line), the black line is the expected value of the model, the red line is the lower 95% prediction limit, green line is the F_b; horizontal dashed lines correspond to values at the given level of predicted *MOR*

Once a model for predicting *MOR* is established and a lower 95% prediction limit is calculated for each level of predicted *MOR*, the allowable F_b may be calculated. Figure 4.10 shows the plot of generated samples from the distribution parameter estimates in Table 4.17, though it could be from any prediction model for *MOR* and other distributions. The black trend line running through the data is the expected value from the model; that is, the value of the predicted *MOR* from the regression model. The red line is the lower, one-tailed 95% prediction limit, which can be calculated from Equation 4.11. Below the red prediction limit line is a green line, which is the lower prediction limit, divided by 2.1, the factor of safety; this is the allowable F_b. For a given level of predicted *MOR* from the model (blue vertical line intersecting the data), this corresponds to three unique values: the mean or expected value, the lower 95% prediction limit, and the allowable F_b.

4.6 References

Divos, F. and T. Tanaka. 1997. Lumber strength estimation by multiple regression. *Holzforschung*. 51(5): 467-471.

Forest Products Laboratory (FPL). 2010. Wood handbook – wood as an engineering material. General Technical Report FPL-GTR-190. Madsion, WI: U.S. Department of Agriculture, Forest Service, Forest Products Laboratory.

JAS. 1991. Japanese agricultural standard for structural softwood lumber. SIS-19. Japan External Trade Organization.

Oh, J. K., K. M. Kim, J. J. Lee. 2010. Use of adjacent knot data in predicting bending strength of dimension lumber by x-ray. *Wood Fib. Sci.* 42(1):10 – 20.

5. DISCUSSION

5.1 Overview

This study has twofold significance: (1) it confirms the ability to accurately predict structural lumber with stress waves and minimal visual measurements; and (2) it is one of the few publicly accessible methods to predict static modulus of elasticity and modulus of rupture of southern pine lumber in the explicit context of the grading process. Currently, the methods used by industrial southern pine manufacturers to nondestructively evaluate southern pine lumber are proprietary, but this study provides a reasonable estimate of just how it may be done, and introduces visual measurements that may improve the current grading process. The study demonstrated the implementation of these methods through decision making rules in a simulated grading process and examined the feasibility against the American Lumber Standards Committee grading policy and using National Design Specifications® machine-evaluated grades.

5.2 Visual Parameters

The grid system used to quantify the general location and size of knots was effective as an explanatory variable for MOE_s and *MOR*. As explained in Chapter 3.2.2, each face of each section of the grid is assigned a value of "0" if there is no knot or "1" if a knot greater than ¼-inch is present. The column/row variables (Row_1, Row_2, etc.) are the sum of these values in the particular column/row. Only Row_i variables were used in the analysis since $Column_j$ resulted in uninterpretable or insignificant results.

In the final combined models, the correlation of individual knot variables with MOE_s and *MOR* is fairly high (Table 5.1). Knots in the center of the board (Row_4, the neutral axis) contribute much less to the explained variation in mechanical properties than knots near the edges. The coefficient of determination is at a minimum in Row_4 and increases toward the edges, Row_1 and

Row7. This is an expected result but arrived in a slightly different manner in that the exact knot sizes and locations were not measured. Unlike other studies, the focus here is not on determining this exact relationship between knot size, knot location, and mechanical properties, but rather finding a loosely theoretical, approximate solution that can be immediately used in the lumber grading process. The effect of knots are slightly greater on strength than on stiffness perhaps because of a "weakest link" phenomenon. Stiffness may result from a cumulative effect of knots rather than strength which is dictated by the region with the most defects which reduced the allowable load of the entire sample.

Table 5.1 – R^2 of row variables with MOE_s and *MOR* for the combined sets with influential samples removed

ΣRow_i	R^2 (MOE_s)	R^2 (*MOR*)
Row_1	0.189	0.249
Row_2	0.192	0.191
Row_3	0.102	0.142
Row_4	0.055	0.083
Row_5	0.105	0.197
Row_6	0.124	0.291
Row_7	0.127	0.303

The knot area ratio (KAR) and other techniques that measure the ratio of the cross-section occupied by knots, though accurate, are often difficult to measure in practice since only the external knot can be measured. More sophisticated methods such as x-rays must be used to obtain internal images of knots. Oh et al. (2008; 2009; 2010) used X-rays to image internal knots to predict the bending strength. Oh et al. (2010) reported R^2 values between 0.50 and 0.60 for predicting the bending strength of Japanese larch and red pine boards 38 mm thick by 140 mm wide by 3.6 m long (1.5 in. x 5.5 in. x 11.8 ft.). Compare these results to the following models that contain only row variables (Table 5.2). An R^2 of 0.562 can be achieved with just four visual

variables that only require external measurements of knots and the limited calculations of row summation variables. There needs to be no explicit mention of edge knots and there are also no assumptions of the internal knots based on external observation.

Table 5.2 – Predictive models for *MOR* using knot variables only for combined sets with influential samples removed

MOR Prediction Model Parameters[a]	R^2	Mean Square Error	Predicted Sum of Squares ($x10^8$)
β_0 = 7,284 β_1 = - 436 β_7 = - 453	0.452	3,462,211	4.949663
β_0 = 7,976 β_1 = - 343 β_3 = - 408 β_6 = - 762	0.535	2,958,082	4.263803
β_0 = 7,969 β_1 = - 320 β_3 = - 395 β_6 = - 507 β_7 = - 233	0.562	2,807,515	4.060207

[a] β_0 = intercept parameter, β_1 = Row_1 parameter, β_3 = Row_3 parameter
β_6 = Row_6 parameter, β_7 = Row_7 parameter

The dichotomous nature of each grid ("knot present" or "knot absent") combined with the fairly large cell sizes may seem to be overly simplistic. In certain cases, the 3 in. x ¾ in. grids lack the resolution necessary to accurately describe the location and true size of the knots. Two equally-sized knots could produce very different results depending on its location relative to the grid (Figure 5.1). One improvement may be to decrease the size of the cells so that when summed, the Row_i variables are closer to the true amount occupied by knots. The magnitude of improvement would be dependent upon the change in size of the grids and the frequency of the situation in Figure 5.1. Given that the results with relatively large cells are satisfactory and the unlikeliness

that a board would only contain knots like that illustrated in Figure 5.1, it may be unnecessary to drastically change the cell size. The average size of knots would likely affect the optimum size of the cells, also.

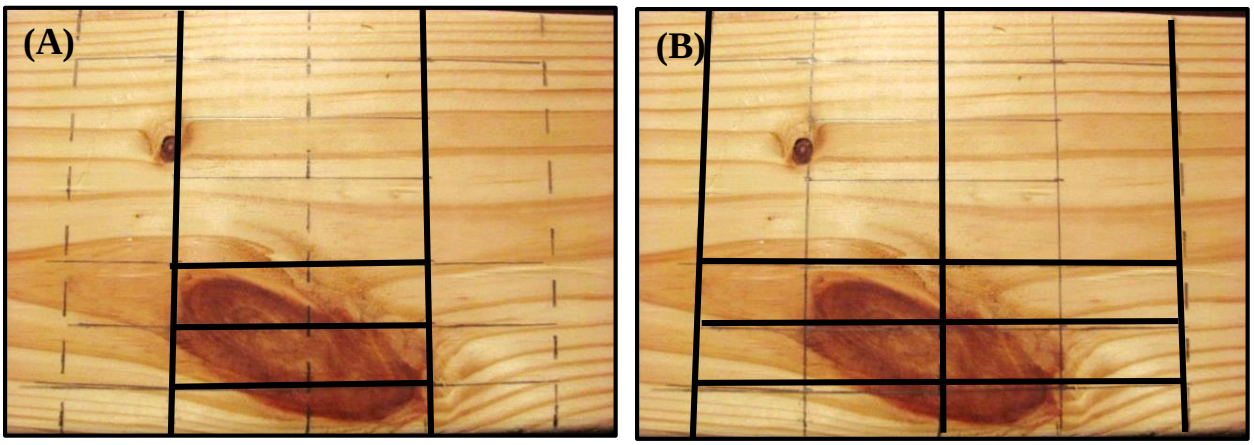

Figure 5.1 – Example of how the varying grid locations can drastically change the knot variables; (A) knot would result in three defective cells, (B) knot would register as six cells

If the cell width were to be changed, this would likely lead to multicollinearity problems in the regression. With the current dimension of ¾-inch wide cells, the row variables have fairly high correlation with each other in adjacent rows which range from 0.523 to 0.716 (Table 5.3); rows that are not adjacent are much less correlated as they are further away and do not share knots. Even with relatively high correlation, it is not enough to cause multicollinearity in the regression which allows each row variable to be used as a predictor variable in the regression without damaging the predictive capability of the model. The main cause for this high correlation between adjacent rows is knots that cross into both rows, although some could be attributed just from being part of the same board. In order for a single knot to be in only one row, it would have to be no larger than the cell width and located in the row such that it doesn't cross into the adjacent row; this would require a knot no larger than ¾-inch (or the specified row width) and perfectly within the row. As a result

of this, adjacent rows are somewhat interchangeable in most of the models. This is most likely the cause for unexpected models that may contain Row_1 and Row_3, but not Row_2.

Table 5.3 – Correlation matrix of row variables for combined training and validation sets, excluding influential samples

	Row_1	Row_2	Row_3	Row_4	Row_5	Row_6	Row_7
Row_1	1.00	0.654	0.345	0.178	0.128	0.174	0.224
Row_2		1.00	0.682	.260	-.010	0.019	0.125
Row_3			1.00	.523	0.066	-0.047	0.036
Row_4				1.00	0.533	0.209	0.091
Row_5		*Symmetric*			1.00	0.641	0.339
Row_6						1.00	0.716
Row_7							1.00

Suppose that each row was divided into smaller increments to achieve better precision in measuring knots. As the width approaches zero, the summation of rows that contain a knot will converge to the actual width taken up by the knot. However, as the cell width decreases, adjacent rows become more alike because they contain the same knot. As a result, most of the row variables would become useless since only the rows near the edge of knot contain new information. This method of knot measurements is deliberate in order to account for another complex factor that affects wood strength: slope of grain. It is well known that knots are one of the main causes for slope of grain in lumber which significantly decreases the bending strength and stiffness. Since no rapid and accurate technique of measuring slope of grain was available for use, the knot variables were developed in part to account for local deviations in the slope of grain due to knots.

By allowing cells that contain any non-trivial amount of knot to be categorized as defective – a value of one in the knot summation variable – this indirectly measures slope of grain due to knots. Since slope of grain extends around the knot, large cells that may only contain a small amount of a knot will likely contain sloped grain that reduces strength (Figure 5.2). In the figure, the cells that contain just a small amount of knots (as indicated by the arrows) also have localized slope of grain. If the cell size were reduced to increase the accuracy of measuring the actual knot

size, it would not capture the effect of slope of grain in many cases. In this method of using large cells, the knot is treated as a localized region of weakened material that extends some distance around the actual knot; the effect of knots and slope of grain, therefore, are indistinguishable from one another.

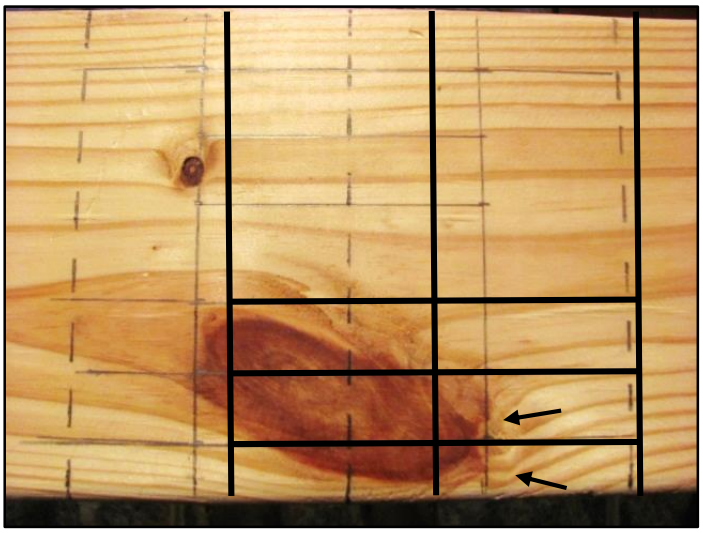

Figure 5.2 – Example of small amount of knots in cells that also accounts for localized slope of grain as indicated by the arrows

5.3 Final Regression Models

The final regression models for MOE_s and *MOR* were built using the original training set of 82 samples (Chapter 4.2), validated with an independent, external set of 58 samples (Chapter 4.3) then refit using the combined training and validation sets to tune the regression parameters (Chapter 4.4). In each of the data sets, influential samples were removed from the analysis. The total proportion of removed samples is about 0.06 of the combined sets, or only nine from a total of 149 samples.

As previously mentioned, one wavespeed measurement of 18,000 ft/s or greater was a unique trait in these influential samples that was not found in the others. Density and knot measurements for the influential samples were similar to normal samples and did not raise concern.

However, the minimum rings per inch of these influential samples tended to be quite low – each was below the overall average of 4.5 rings per inch - but not every sample with low rings per inch had abnormal wavespeed and was influential. Although rate of growth measurements ($Ring_{min}$ and $Ring_{ave}$) are not used in models that removed influential samples (Chapters 4.2 and 4.4), its inclusion significantly improves the performance of models that include all boards (Chapter 4.1). This indicates that abnormal wood formation that results in wide rings may be the cause of the unusual wavespeed. Most likely growth defects such as compression or juvenile wood are the cause. In both compression and juvenile wood, the tracheid and cell wall structure is significantly different than that of mature, normal wood, thus capable of causing unexpected wave behavior and reduced mechanical properties.

Although the exact cause of these higher wavespeeds is unknown – and for the purposes of this study, relatively unimportant – it can be used as a cutoff value to remove unpredictable samples when predicting mechanical properties from dynamic modulus of elasticity. The specific wavespeed may be unique to the equipment used in this study, but the general idea of a wavespeed threshold may be applied in the lumber grading process. Calibration would likely be required for different equipment and species, or even dimensions and moisture contents. Indicator variables could be added to the current regression equations or entirely new models could be developed for samples that contain higher wavespeeds in order to accurately predict mechanical properties of these samples. As the quality of available lumber decreases due to increased reliance on rapidly-grown, small diameter trees, models that can adequately account for poor wood quality will be advantageous. The potential of such a screening process and the advantage of machine grading is illustrated in the validation set that contained 60 visually-graded samples: the two samples with wavespeeds greater than 18,000 ft./s that were removed were of visual grad No.1. These samples

met all visual grading criteria of a No.1 grade, yet were far below adequate stiffness. Although there is tolerance by way of lower 5% limits within a grade, the elimination of such clearly poor pieces would reduce the variability within a grade.

5.3.1 Final Static Modulus of Elasticity Model

The final MOE_s model (Equation 4.5) is a simple three parameter model, plus an intercept term and is very similar to the original model using the training set (Equation 4.3). As expected, the density and average wavespeed parameters have positive coefficients; as density and wavespeed increase, the estimated MOE_s also increases. The single visual variable parameter, Row_7, has a negative coefficient of – 31,870. In other words, for every cell face in the outermost bottom row that contains a defect (for every increase of one unit of Row_7), the predicted MOE_s will decrease by nearly 32,000 psi. This difference may seem trivial given a typical board is graded at about 1,500,000 psi, but that is certainly enough to reduce the grade of a board by one or more grades. Naturally, the question may arise of how much more value could be gained by simply specifying which way to place the board such that less knots are on the tension side. This issue will be explored in detail later.

5.3.2 Final Modulus of Rupture Model

The final modulus of rupture model (Equation 4.6) uses predicted MOE_s from Equation 4.5 as well as four knot summation variables – Row_1, Row_3, Row_6 and Row_7. Since the parameter estimate of predicted MOE_s is positive, the predicted *MOR* increases with the predicted value of stiffness. Each of the knot parameters is negative which causes the predicted *MOR* to decrease as the value of knots increase. The results are generally intuitive, yet the parameter estimates may not be easily explained. The similarity of knot variables in adjacent rows is the cause for the inclusion of some rows yet not others.

The parameter estimates of Row_6 and Row_7 are -352 and -162, respectively. Knots in Row_6 have more than twice the effect on predicted bending strength than Row_7 even though the region closer to the edge – Row_7 – has greater internal stress (Figure 3.4). This may be explained by the prediction equation for MOE_s, in which Row_7 is already included. Some of the effect of knots in the outer tension region is already accounted for, resulting in reduced predicted MOE_s and thus a lower predicted *MOR*.

It is not completely clear, however, why the effect of knots near the neutral axis in Row_3 reduce the predicted *MOR* greater than knots in the outer compression edge, Row_1. This does not follow expected results based on internal stress distribution. When individual knot variables are regressed with *MOR* for the training set (Table 4.1), it results in the expected effect of knots on bending strength – greatest effect on the edges with tension side more significant and minimum correlation at the neutral axis. It was also shown that adjacent rows are more correlated due to knots that are in both rows (Table 5.2). It is likely that Row_3 reduces the predicted *MOR* more than Row_1 since it is adjacent to two rows rather than just one. In a way, Row_3 carries with it the effect of both its adjacent rows, whereas Row_1 has just one adjacent row. Since Row_3 also contains most of the knots that are in Row_2 and Row_4, this may lead to greater significance.

5.4 Grading Simulation

5.4.1 Static Modulus of Elasticity Grading

The primary purpose of the simulation study presented in Chapter 4.5.2 is to illustrate the plausibility of using the regression equations for predicted MOE_s for grading. The actual parameter distributions are most likely different than those estimated based on the 140 samples, but the procedure would be similar. The accuracy of the models, or the distribution of the residuals, should be the focus as this is the critical measure of their usefulness. For any distribution of predicted

MOE_s, the average E for any range of values can be calculated as in Equations 4.7 through 4.11, with equations 4.7 through 4.9 depending on the distribution and equations 4.10 and 4.11 depending on the characteristics of the model, i.e. the relationship between the predicted and actual MOE_s.

As mentioned in previous chapters, one of the two requirements of a machine grade is that boards in a given grade have an average MOE_s of that which is specified in the grade. This is relatively easy to accomplish, no matter how well the model performs. One of the characteristics of least-squares regression is that residuals – the difference between the actual value and the predicted value – have a mean of zero. The expected value of the model, or the average value over a large number of samples, is the regression line – the predicted value of MOE_s at every level of input variables. Because of these properties, the average value of a distribution function of random variables (as in Equation 4.7), in this case the predicted MOE_s, will be the average values of the expected values of the regression equation. The magnitude of the residuals of the regression model has no bearing on the average value of the distribution since they have mean of zero. So, if an alternative method of prediction was used, the method of grouping based on average value of the distribution would be unaffected. The second requirement of machine-grade lumber does require special attention to the variance of the model in addition to the distribution.

The second requirement, E_{min}, is related to the variability of the errors from the predictive model as well as the variability of the distribution. The total variability within a grade bin is the variability from the model (i.e. the residuals) and variability of the interval on the distribution since each bin contains a non-uniform distribution of values (Figure 5.3). Therefore, wide bins that contain a larger interval of predicted MOE_s will have higher variance than narrow bins. The location of the interval will also affect the total variance within a bin as the probability density

changes. Bins that are located over an interval that rapidly changes will have greater variance than those that are over more uniform intervals on the distribution.

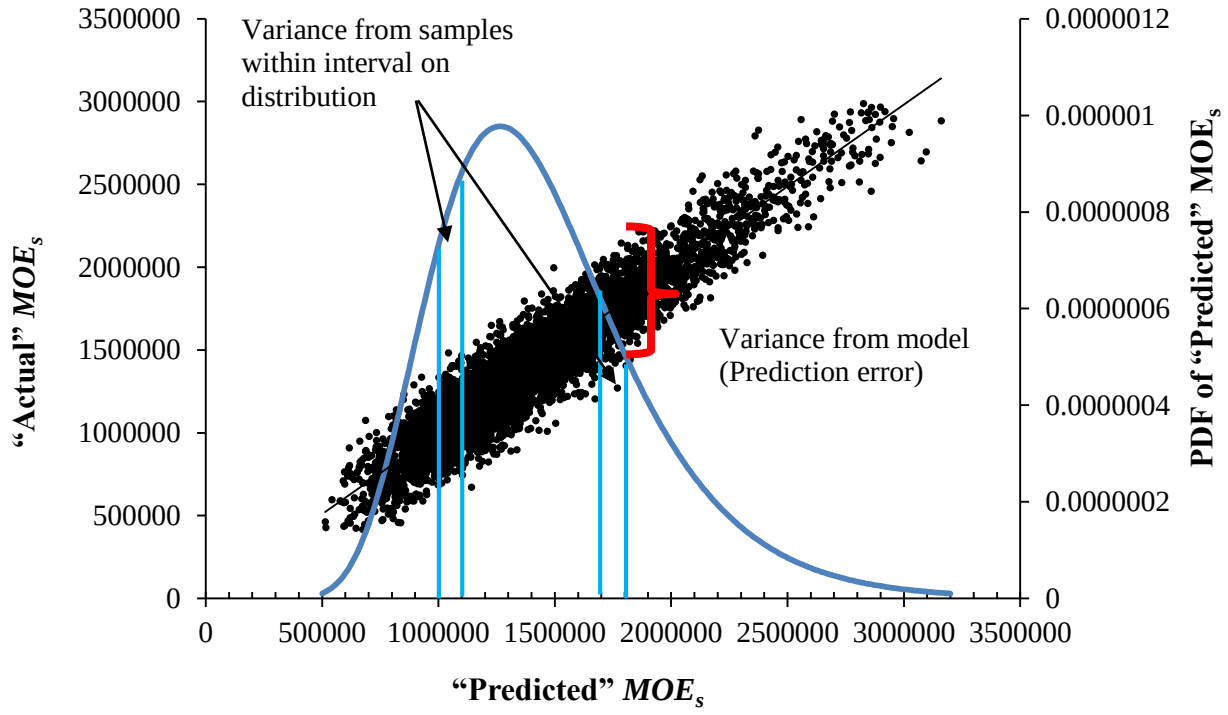

Figure 5.3 – Randomly generated samples following the distribution parameters in Table 4.12 for predicted MOE_s and its overlaid probability density function (PDF); horizontal lines show intervals of equal width that would produce different variance; red brackets show the constant variance from the model

To illustrate this principal, a moving standard deviation for groups of various sizes of the randomly generated samples was calculated (Figure 5.4). Samples were arranged in increasing sequential order of "predicted" MOE_s and the standard deviation of "actual" MOE_s was calculated in a moving fashion such that the number of samples in each calculation was 100, 500 and 1,000 for each group. Beginning with sample 100, the standard deviation of the previous 100 samples was calculated, then sample number two to 101 and so on until the last sample that was included in a bin from Table 4.18 was reached. This was done for the 500 and 1,000 sample groups starting with sample 500 and 1,000, respectively. The position in the distribution (sample number) and the width of the interval greatly affect the standard deviation.

A theoretical total variance could be calculated on any interval for any distribution, but this is unnecessary for the purpose of this study. Since the simulated sample standard deviation in the bins are fairly constant and include just 5,000 samples, calculating the total variance from a distribution and model variance would likely prove very little and may not necessarily be close to the simulated value. The bin-to-bin variance in this simulation study is likely dominated by the variance due to prediction errors (i.e. sample to sample variation) and not the variance due to the bin interval and its position within the distribution; even hundreds of samples will not converge to the true total variance.

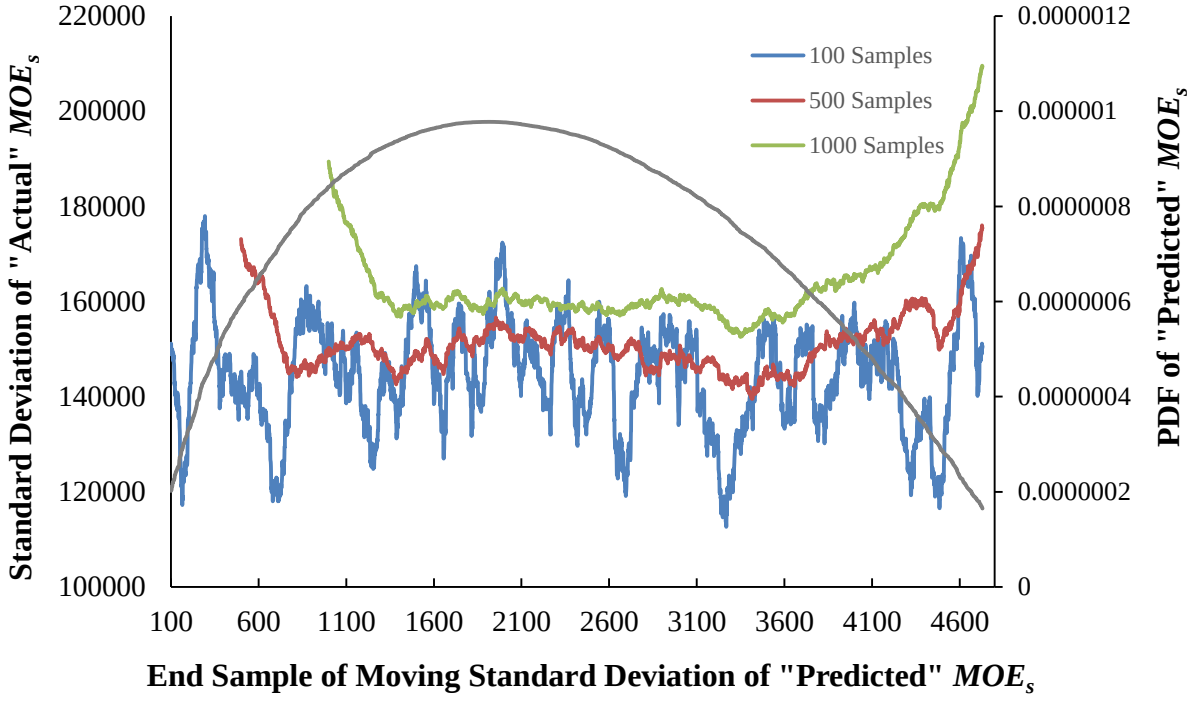

Figure 5.4 – Moving standard deviation of "actual" MOE_s depending on sample size and location within distribution of "predicted" MOE_s; probability density function (PDF) of distribution of "predicted" MOE_s

Thousands of samples would be needed in individual grade bins to achieve convergence with the true variance. Also, interval widths of only 100,000 would likely make this value small. However, for an actual lumber grading process that deals with hundreds of thousands of samples,

this may be of interest. In this case, the second central moment of the distribution over the specified interval would be added to the prediction variance. If the true variance was known for any interval, the optimum interval to meet the requirement of 95% of samples greater than or equal to 75% of assigned *E* could be met with greater efficiency.

It can be seen from Table 5.4 that the relationship between 75% of the average *E* and the average *E* itself changes linearly as the grade increases. For 95% of pieces within a grade to be above 75% of average *E*, a linear increase is tolerated in the maximum allowable standard deviation of the samples within the grade as the grade level increases. This implies that the current models used to predict MOE_s may not have homogeneous variance, but may "fan out" as levels of the predicted MOE_s increase. Although the sample is size more than adequate to develop regression equations and parameter estimates, this may indicate that more samples are needed, especially at higher levels of predicted $MOE_{s,}$ to fully develop a grading procedure in accordance to the current design specifications. This tolerance for increased variance also allows the total bin variance to increase as the grade level increases, which is related to the distribution.

It is also possible that the developed method is more accurate than those currently used and may have another advantage in that that residuals are homoscedastic. This would be advantageous for many reasons, especially in the process of choosing intervals to place boards in the grading process. Likely, for industrial stresswave and visual grading systems, some accuracy is compromised for processing speed. As of now, it is impossible to conclude that the developed model is superior without testing more samples and knowing the limitations of industrial grading processes, although it is promising.

Table 5.4 – Maximum standard deviation by grade to achieve requirement of 95% of pieces greater than 75% *E*

Average *E*	Required 75% of Average *E*	Maximum Grade Bin Standard Deviation (Assuming average *E*)
1,000,000	750,000	151,976
1,100,000	825,000	167,173
1,200,000	900,000	182,371
1,300,000	975,000	197,568
1,400,000	1,050,000	212,766
1,500,000	1,125,000	227,964
1,600,000	1,200,000	243,161
1,700,000	1,275,000	260,283
1,800,000	1,350,000	273,556
1,900,000	1,425,000	288,754
2,000,000	1,500,000	303,951
2,100,000	1,575,000	319,149
2,200,000	1,650,000	334,347

5.4.2 Modulus of Rupture Grading

The modulus of rupture grading process is similar to the modulus of elasticity grading process with one exception: allowable bending stiffness does not require an average value for any grade, as explained in Chapter 4.2.2. As a result, the distribution of the predicted *MOR* seems largely irrelevant in the actual grading process, and is only used in this study to simulate several thousand samples in order to put the models into the context of actual grades. The assigned bending stress, F_b, is similar to that of E_{min} in that it requires a certain percentage of pieces within a grade to exceed a minimum value after a factor of safety is applied. The critical component is the distribution of the residuals, or the mean squared error of the prediction model. This will determine how useful the models are in the grading process. Since the allowable bending stress is not constrained by an interval within the distribution, just a simple prediction limit for any level of predicted *MOR* will correspond to an allowable bending stress.

Much of the procedure has already been discussed in Chapter 4.2.2 but it must be emphasized that mean squared error of the model should be minimized in order to create narrower prediction limits that will maximize the efficiency of grading.

5.5 Optimization Grading

From the regression equations for predicted MOE_s and MOR (Equations 4.5 and 4.6), it can be seen that knot variables significantly affect the predicted values and thus the grade designation for each board. Since the global parameters of density and wavespeed are fixed for each board, the location of knots would need to be changed to maximize the predicted value, assuming the board is utilized in the specified orientation. This would be achieved by changing the orientation of the board such that knot row variables would maximize the predicted value, i.e. flipping the board.

To maximize predicted MOE_s, the difference in the value of Row_1 and Row_7 are compared and the board should be oriented such that the row with lesser value should be chosen as Row_7. The increase in predicted MOE_s will be 31,780 – the parameter estimate for Row_7 – multiplied by the difference in the values of Row_1 and Row_7. Of the 140 samples used to create the final model in Chapter 4.4, 87 had different values for the two row variables. The average difference between Row_1 and Row_7 for the 87 samples was about three, or nearly a 100,000 psi difference in the predicted MOE_s. Although some boards will not have a true MOE_s that reflects this maximization due to prediction error, the expected or average value of the actual MOE_s at a given level of the predicted MOE_s will be equal to that predicted value since the least squares solution is unbiased with errors that have a mean of zero (Montgomery et al. 2012). In other words, maximizing the predicted value of MOE_s by altering the row variables will necessarily maximize the average actual MOE_s.

Simply specifying the orientation of the board could maximize predicted and, therefore, actual MOE_s, in some extreme cases by as much as 380,000 psi. This would directly lead to an improvement in grade and would optimize the potential of each board. However, it would require the specification of the proper orientation of each board in bending. This may be something lumber producers are unwilling to do and may complicate design specifications. It may be possible to specify two values of stiffness – a minimum and a maximum, dependent upon which side is loaded in compression or tension. Within each 100,000 psi grade-range of *E*, another value could be specified for each board – maximal stiffness as determined by orientation. Each board would be graded based on the minimum predicted MOE_s for both orientations. Then, the maximum MOE_s would be specified along with the proper orientation.

The optimization of bending strength is similar to that of stiffness, but is slightly more complicated because (1) it depends on the predicted MOE_s, which may take two values; and, (2) there are four knot variables that must be considered, rather than just two. Maximizing the predicted MOE_s may not necessarily maximize predicted *MOR* for the same board since the values of the other row variables could result in lower predicted values of *MOR*. In practice, a board would have two values of predicted MOE_s and *MOR* – one set for each orientation. A lumber producer could choose which parameter to maximize based on the predicted value of strength and stiffness for each of the two orientations. Fortunately, when the orientation is chosen such that MOE_s is maximized, the *MOR* is also maximized much of the time. Of the 140 samples, 79 had both maximum predicted MOE_s and *MOR* for the same orientation with only 11 with maximum predicted values of one parameter under one orientation and a maximum of the other predicted parameter under the other orientation (Table 5.4). Many of the samples had identical predicted MOE_s for both orientations because only the outer row knot variables (Row_1 and Row_7) must be

identical, which is not uncommon. Similarly, if the orientation is chosen such that the predicted *MOR* is maximized, then 129 of the 140 samples (92%) had maximum predicted MOE_s, but this would require each of the predicted MOE_s to be calculated beforehand.

For instance, orientation A could have predicted MOE_s of 1,200,000 psi and predicted *MOR* of 5,000 psi and orientation B have predicted MOE_s of 1,100,000 psi and predicted *MOR* of 6,000 psi. Depending on how the board is used (i.e. the orientation during bending), the allowable mechanical properties may vary considerably just by flipping the board, though they are usually maximized with the same orientation.

Table 5.5 – Optimization summary of 140 samples when orientation is chosen to maximize predicted MOE_s if two unique values exist or when they are equal

Orientation Criteria	*MOR* Maximized	*MOR* Minimized
Maximum MOE_s	79	11
	MOR Identical	*MOR* Different
MOE_s Identical	21	32

For any knowledgeable user of lumber, it is common sense to avoid knots on the tension side when loaded in bending, especially near the edge. This principal may not always be followed in practice and unless explicitly marked, it would be unreasonable, if not impossible, to estimate the difference between orientations for a particular board. However, the exact values, or at least the predicted values that would lead to a particular grade, could be stated for specific loadings and orientations to predict the allowable values under any circumstance. The specific application and design values of a member are most likely known which may make this method feasible. In theory, each board could have extremely detailed specifications for the most common loadings, as well as differences

between orientations. The heterogeneous structure and behavior of wood is a disadvantage that complicates its use; but, as this study highlights, there are methods to overcome this that should be pursued.

5.6 References

Montgomery, D. C., E. A. Peck and G. G. Vining. 2012. Introduction to Linear Regression Analysis, 5th Edition. John Wiley & Sons,

Oh, J. K., K. M. Kim, J. J. Lee. 2008. Development of knot quantification method to predict strength using X-ray scanner. *J Korean Wood Sci Technol*. 36(5):33 – 41.

Oh, J. K., K. M. Kim, J. J. Lee. 2009. Quantification of knots in dimension lumber using a single X-ray radiation. *J Wood Sci.* 55(4):264 – 272.

Oh, J. K., K. M. Kim, J. J. Lee. 2010. Use of adjacent knot data in predicting bending strength of dimension lumber by x-ray. *Wood Fib. Sci.* 42(1):10 – 20.

6. CONCLUSION

Nondestructive physical and visual measurements were used to develop regression models to predict the static modulus of elasticity (MOE_s) and modulus of rupture (MOR) of 2x6, 8 ft. long southern pine lumber. The nondestructive physical measurements included wavespeed and density; visual variables included rate of growth and a developed knot measurement method that also accounts for localized slope of grain. This knot measurement system proved to be an accurate and simplified approach to account for the location and size of knots and the surrounding slope of grain. The dichotomous classification of each cell face within the grid system and the summation of rows reduced a relatively complex system into a form that was readily fed into standard multiple regression.

Two sets of predictive models were developed: one set which included all samples and another that did not include boards with wavespeeds greater than 18,000 ft./s as these were very influential to the model. The models that included all samples were inferior to the modes that did not include the influential samples. The dynamic modulus of elasticity calculated from density and wavespeed, which is the standard approach for predicting MOE_s, was not valid for samples that had abnormally high wavespeeds, which this method useless for sample sets that included the influential samples. Instead, the rate of growth as measured by minimum rings per inch of both ends, as well as density and knot variables, was used to predict MOE_s and MOR. The coefficient of determination for the models in the training set for predicted MOE_s and MOR was 0.712 and 0.690, respectively. However, since the proportion of samples that had abnormal wavespeeds was relatively low and those samples were of very poor quality anyway, models that excluded the influential samples became the focus of the study.

Models with influential samples removed performed better than those that included all samples – R^2 of 0.892 and 0.714 for MOE_s and *MOR*, respectively. Unlike the models that included all samples, these models did not include ring measurements which are difficult to measure and are most likely imprecise. These models performed better with independent samples (the validation set) which implies better predictive performance. As demonstrated in the simulated grading study, these models have adequate performance to meet the American Lumber Standards Committee (ALSC) criteria for machine-evaluated lumber (MEL).

Both sets of models include the developed knot summation variables derived from the grid system. For both models, the effect of knots on MOE_s and *MOR* was shown to be very significant, especially for *MOR*. As expected, the amount of knots as well as their location is significant. The method of measuring knots was effective, although some modification to the size of the grids may be necessary. Future studies may eliminate interior rows altogether and slightly reduce the width of outer rows to increase the accuracy. This method may eventually evolve into more than simply summing rows of knots, perhaps by dealing with individual cells, their locations, and the possible interaction between them.

This study suggests that simplified approaches to account for defects in lumber may be used without sacrificing predictive ability. The method of segmenting the board into cells and simply classifying as "defective" or "non-defective" may have advantages in the current lumber grading procedure. For one, visual scanning systems may detect binary outcomes for specific regions more accurately and quickly. Summing the number of defective cells may be less computationally intensive than other methods, also. If cell dimensions are chosen correctly, slope of grain is accounted for which currently is measured with much more involved methods.

A grading simulation study was carried out in order to test the feasibility of the developed models to adhere to actual southern pine design specifications. Distributions were estimated from the samples and 5,000 random samples were generated according to the estimated distribution parameters. The models performed very well and sorted the generated samples into grades in compliance with the American Lumber Standards Committee policy for machine-evaluated lumber. Details of the grading procedure were also explained such that MOE_s and *MOR* lumber grading would be better understood.

As a result of the developed predictive models, changes to design specifications for southern pine structural lumber were suggested in which each orientation of the board would be assigned an allowable bending stress and stiffness. The location of knots as measured by Row_i variables is dependent upon the orientation of the board; thus it is possible to maximize the predicted and, therefore, actual mechanical properties by changing the Row_i variable. Liability issues and difficulties of implementation aside, the specification of the optimal orientation of each board could be very beneficial. Not only would producers be able to maximize the value of each board by increasing the allowable load and its grade, but the resource would be used more efficiently. The value to not only the producer, but the user of lumber may greatly increase if these opportunities are explored.

THE VITA

Jacob Romer is a native of central New York from the town of Canastota. He received his bachelor's degree from the State University of New York College of Environmental Science and Forestry in 2011 and entered graduate school at Louisiana State University the following year. His technical interests include the nondestructive evaluation and grading of lumber.